

¹ AWmeta empowers adaptively-weighted transcriptomic meta-analysis

³ **Yanshi Hu**  ^{1,*}, **Zixuan Wang** ¹, **Yueming Hu**  ¹, **Cong Feng** ^{1,2}, **Qiuyu Fang** ³, and **Ming Chen**  ^{1,2,*}

⁵ ¹Department of Bioinformatics, College of Life Sciences, Zhejiang University, Hangzhou 310058, China

⁶ ²Biomedical Big Data Center, The First Affiliated Hospital, Zhejiang University School of Medicine; Institute of
⁷ Hematology, Zhejiang University, Hangzhou 310058, China

⁸ ³Department of Thoracic Surgery, The Second Affiliated Hospital Zhejiang University School of Medicine, Zhejiang
⁹ University, Hangzhou 310058, China

¹⁰*Corresponding author email(s): yanshihu@zju.edu.cn; mchen@zju.edu.cn

¹¹ ABSTRACT

Transcriptomic meta-analysis enhances biological veracity and reproducibility by integrating diverse studies, yet prevailing *P*-value or effect-size integration approaches exhibit limited power to resolve subtle signatures. We present AWmeta, an adaptively-weighted framework that unifies both paradigms. Benchmarking across 35 Parkinson's and Crohn's disease datasets spanning diverse tissues and adaptively down-weighting underpowered studies, AWmeta yields higher-fidelity differentially expressed genes (DEGs) with markedly reduced false positives and establishes superior gene differential quantification convergence at both gene and study levels over state-of-the-art random-effects model (REM) and original studies. AWmeta requires fewer samples and DEGs from original studies to achieve substantial gene differential estimates, lowering experimental costs. We demonstrate AWmeta's remarkable stability and robustness against external and internal perturbations. Crucially, AWmeta prioritizes disease tissue-specific mechanisms with higher functional coherence than those from REM and original studies. By bridging statistical rigor with mechanistic interpretability, AWmeta harmonizes heterogeneous transcriptomic data into actionable insights, serving as a transformative tool for precision transcriptomic integration.

¹³ Main

¹⁴ The exponential expansion of publicly available transcriptomic data, propelled by high-throughput sequencing advancements¹,
¹⁵ presents unprecedented opportunities and concomitant challenges for uncovering robust biological insights through meta-
¹⁶ analysis. By integrating findings across independent studies, this powerful approach transcends the limitations of individual
¹⁷ datasets, mitigating issues of statistical power, experimental variability, tissue heterogeneity, and platform-specific biases that
¹⁸ often obscure subtle yet pathologically relevant expression signatures^{2,3}. As complex diseases increasingly defy dissection by
¹⁹ single-study designs, meta-analysis has become indispensable for identifying reproducible biomarkers and elucidating disease
²⁰ pathways with enhanced confidence and precision^{4,5}.

²¹ Contemporary meta-analysis methodologies predominantly fall into three primary categories⁶: *P*-value combination,
²² effect-size integration, and rank aggregation. *P*-value-based methods, such as Fisher's⁷, Stouffer's Z-score⁸, and the adaptively
²³ weighted Fisher's (AW-Fisher) technique⁹, efficiently aggregate statistical significance but typically disregard effect magnitude
²⁴ and directionality. Conversely, effect-size approaches quantify expression differences, with the random-effects model (REM)¹⁰
²⁵ widely adopted due to its capacity to accommodate inter-study heterogeneity and its perceived biological interpretability¹¹.
²⁶ REM has underpinned discoveries in diverse areas, including characterizing gut microbiome dysbiosis in Parkinson's disease¹²,
²⁷ identifying predictive biomarkers for cancer immunotherapy¹³, and assessing pharmacogene expression in nonalcoholic fatty
²⁸ liver disease¹⁴. Nevertheless, REM and related models can exhibit sensitivity to outlier studies and rely heavily on assumptions
²⁹ about the underlying heterogeneity structure^{11,15}. Rank-based techniques (e.g., RankProd and RankSum^{16,17}) offer robustness
³⁰ against outliers but often at the cost of statistical resolution and power. Critically, these distinct methodological frameworks
³¹ typically operate in isolation, failing to synergistically leverage their complementary strengths.

³² This methodological schism represents a fundamental constraint in transcriptomic meta-analysis, particularly impeding
³³ progress in complex disease research where robust biological inference demands both high statistical confidence in identifying
³⁴ dysregulated genes and accurate quantitative estimates of their expression changes^{18,19}. Current *P*-value integration schemes,
³⁵ while adept at pinpointing consistently altered genes, offer minimal information on the magnitude or biological relevance of
³⁶ these alterations. Conversely, effect-size methods, though designed to quantify these changes, struggle with the pervasive

37 heterogeneity inherent in pooling diverse experimental designs, tissue sources, or patient cohorts, potentially diminishing the
38 estimate reliability²⁰. Furthermore, existing approaches lack sophisticated mechanisms to dynamically weight studies based on
39 intrinsic data quality or specific biological context, thereby limiting overall sensitivity and the depth of achievable insights.

40 To address these critical gaps, we introduce AWmeta, a novel meta-analytic framework that unifies the statistical rigor
41 of *P*-value-based method with the quantitative power of effect-size paradigm. The core innovation of AWmeta lies in an
42 adaptive weighting scheme that (1) identifies and up-weights the most informative studies from a heterogeneous pool, and
43 (2) explicitly models between-dataset variability to mitigate bias arising from sample size imbalances, data sparsity, and
44 technical heterogeneity. Validated on 35 diverse transcriptomic datasets spanning Parkinson's and Crohn's disease across
45 multiple tissues, AWmeta consistently outperforms the state-of-the-art REM. It secures higher-fidelity differentially expressed
46 gene (DEG) identification with markedly reduced false positives, exhibits greater resilience to limited sample size and DEG
47 sparsity, and maintains remarkable stability against various perturbations. More importantly, AWmeta delivers gene differential
48 estimates with enhanced reproducibility and biological mechanism interpretation. By reducing sample-size requirements and
49 demonstrating robustness to noise, AWmeta empowers researchers to mine the ever-expanding corpus of public transcriptomic
50 data more effectively, accelerating the discovery of actionable molecular insights across biomedical domains.

51 Results

52 Overview of AWmeta

53 AWmeta is a transcriptomic meta-analytical framework, uniquely synergizing statistical strengths from *P*-value and effect size
54 integration methods (Fig. 1a and "Overview of the AWmeta framework" section in Methods). Following preprocessing of
55 multiple transcriptomic datasets from original studies of the same disease tissue ("Transcriptomic data preprocessing" section
56 in Methods), AWmeta implements two complementary gene-wise modules: AW-Fisher and AW-REM. The AW-Fisher module
57 calculates meta *P*-values by optimizing study-specific weights to minimize the combined probability, effectively filtering out
58 less informative studies while preserving statistical power. Subsequently, in AW-REM module these optimized weights are
59 embedded into REM architecture to derive weighted fold change estimates.

60 In the following sections, we detail a multifaceted rigorous comparison of AWmeta against the state-of-the-art REM, a
61 representative effect-size integration method^{21,22}. Benchmarking on 35 transcriptomic datasets from Parkinson's and Crohn's
62 disease tissues (Extended Data Fig. 1 and "Transcriptomic datasets" section in Methods), this evaluation assessed key metrics
63 including DEG detection capability and discrimination, gene- and study-wise gene differential quantification convergence,
64 stability and robustness, and biological relevance ("Transcriptomic meta-analysis evaluation metrics" section in Methods).
65 AWmeta consistently demonstrated superior performance, establishing its utility as a powerful tool for precision transcriptomic
66 integration and providing a solid foundation for downstream biological investigation.

67 AWmeta secures robust higher-fidelity DEG identification across transcriptomic contexts

68 A primary goal of transcriptomic meta-analysis is to enhance statistical power for identifying DEGs reliably, i.e., to detect
69 more subtle yet vital DEGs, typically defined by statistical significance and fold-change thresholds (Fig. 1b and "DEG
70 detection capability evaluation" section in Methods). Systematically benchmarking across five distinct disease tissue contexts
71 using nine combinations of statistical significance (0.01, 0.05, and 0.10) and fold-change thresholds ($\log_2 1.2$, $\log_2 1.5$, and
72 $\log_2 2.0$), AWmeta consistently identified significantly more DEGs than REM ($P < 10^{-4}$, one-tailed Welch's *t*-test over 100
73 bootstrap iterations; Fig. 1c and Extended Data Fig. 2). For instance, under a specific threshold combination ($P < 0.01$ and
74 $|\log_2 \text{FC}| > \log_2 1.2$), AWmeta yielded 69–475% increases in detected DEGs versus REM across all tissues (Fig. 1c), which
75 demonstrates AWmeta's superior statistical sensitivity in DEG detection.

76 A key challenge in meta-analysis is to increase statistical power while rigorously controlling false positives. To formally
77 evaluate this trade-off, we designed a semi-synthetic simulation framework to assess DEG discrimination ("DEG discrimination
78 evaluation using semi-synthetic simulation strategy" section in Methods). Inspired by Li and colleagues²³, this framework
79 first creates benchmark datasets with a known ground truth of positives (DEGs) and negatives (non-DEGs) (Fig. 1d). We then
80 systematically challenged AWmeta's performance by degrading the biological signal in a controlled manner. This was achieved
81 by permuting sample labels in a progressively increasing number of studies within each tissue context (Fig. 1e). Specifically, we
82 simulated three distinct noise scenarios by permuting the minimum, median, and maximum allowable number of studies, where
83 DEG discrimination was quantified by the area under the receiver operating characteristic curve (AUROC) and the area under
84 the precision-recall curve (AUPRC) over the above defined benchmark genes (Fig. 1f). This perturbation design enabled a
85 rigorous assessment of AWmeta's resilience across diverse data quality landscapes, a critical feature for real-world applications.

86 Across all simulated noise levels, AWmeta consistently outperformed or was comparable to REM in DEG discrimination.
87 Under minimum-permuted low-noise condition, AWmeta demonstrated clear and significant advantage across nearly all tissue
88 contexts and DEG thresholds ($P < 10^{-4}$, 10^{-3} , 10^{-2} or 0.05, one-tailed Mann-Whitney test; Fig. 1g and Extended Data Fig. 3).
89 As expected, performance decayed for both methods with increasing noise from median and maximum study permutations.

90 However, AWmeta's superiority over REM was not only maintained but often became more pronounced under these more
91 challenging conditions ($P < 10^{-4}$, one-tailed Mann-Whitney test; Fig. 1h,i and Extended Data Fig. 4 and 5). Notably, AWmeta's
92 performance remained remarkably robust even under high-noise scenarios, with median AUROC and AUPRC exceeding 0.85
93 in most cases (Extended Data Fig. 5), highlighting its ability to effectively discount noise from potentially confounding studies.
94 Taken together, these results demonstrate that AWmeta achieves a superior balance between heightened detection sensitivity
95 and robust discrimination for higher-fidelity DEG identification from heterogeneous transcriptomic datasets.

96 **AWmeta establishes superior gene- and study-wise convergence in gene differential quantification**

97 To rigorously assess AWmeta's ability to synthesize a consensus biological signal from heterogeneous transcriptomic datasets,
98 we evaluated its convergence at both gene and study levels. We first quantified gene-wise convergence—the proximity of a
99 gene's meta effect-size estimates to ones from original studies—using the mean absolute deviation (MAD) between meta and
100 original fold changes (Fig. 2a and "Gene-wise convergence assessment for gene differential quantification" section in Methods),
101 where lower MADs signify more accurate biological representations.

102 AWmeta consistently yielded significantly lower gene-wise convergence scores in all five disease tissues, compared to both
103 REM and baseline ones (Fig. 2b–f; $P < 10^{-4}$ or 0.05, one-tailed Mann-Whitney test against AWmeta). Notably, while some
104 original studies occasionally outperformed REM in specific contexts, AWmeta (merely 57–74% of REM) consistently achieved
105 lower scores than any original study across all tissues, which suggests its capacity to robustly identify and integrate reliable
106 signals while effectively down-weighting divergent studies, thereby providing a superior consensus representation of the gene
107 expression landscape. Since disease processes are primarily driven by DEGs, we further confirmed this superior performance
108 was still evident for these specific genes by the same assessment paradigm using nine distinct thresholds, combining three
109 significance levels (0.01, 0.05, and 0.10) and three fold-change cutoffs ($\log_2 1.2$, $\log_2 1.5$, and $\log_2 2.0$). Across all threshold and
110 disease tissue scenarios, AWmeta maintained evidently lower convergence scores, accounting for 56–80% of REM (Extended
111 Data Fig. 6a–e; $P < 10^{-4}$, 10^{-3} , 10^{-2} or 0.05, one-tailed Mann-Whitney test over AWmeta), which underscores AWmeta's
112 effectiveness to derive robust fold-change estimates for disease-relevant genes, independent of specific statistical criteria.

113 Next, we evaluated study-wise convergence to determine how well the meta-analytic results reflect the collective evidence
114 across all contributing studies. We employed three complementary approaches: an adjusted rank-sensitive similarity metric
115 emphasizing top-ranked genes (denoted "adjusted DE list similarity" thereafter), the arithmetic mean of Jaccard and overlap
116 coefficients (JC/OC) for DEG concordance, and the phi coefficient (PC)²⁴ to assess classification agreement beyond chance
117 (Fig. 2g–j, Extended Data Fig. 7 and "Study-wise convergence assessment for gene differential quantification" section in
118 Methods). Higher scores indicate better study-wise convergence for all metrics.

119 Across the five disease tissues, AWmeta consistently achieved significantly higher study-wise convergence scores than
120 baselines representing original inter-study agreement, with dramatic 30–1,166% improvements (Fig. 2k–m; $P < 0.05$ and
121 $|\log_2 FC| > \log_2 1.2$ where applicable). While overall convergence scores tended to be lower in Parkinson's over Crohn's
122 disease tissues, potentially reflecting higher inherent variability within these specific disease contexts, AWmeta significantly
123 outperformed REM in the majority (10 out of 15) of comparisons across different metrics and tissues, performing comparably
124 otherwise, particularly pronounced in tissues like Parkinson's and Crohn's peripheral blood, where AWmeta's convergence
125 scores improved by 35–156% compared to REM (Fig. 2k–m). To further validate these findings for the JC/OC and PC metrics,
126 we confirmed AWmeta's superior performance across nine different DEG cutoffs (Extended Data Fig. 8). These results indicate
127 that the gene differential quantification results processed by AWmeta are more representative of the faithful consensus signal
128 across studies than those derived from REM or original studies.

129 **AWmeta attains accelerated meta-analysis convergence with reduced samples and DEGs**

130 While large sample sizes are known to enhance transcriptomic differential quantification efficacy, the feasibility of achieving
131 reliable meta-analytic effect sizes from studies with limited samples has remained an open question. To fill this gap, we
132 systematically correlated study-wise convergence with sample size and employed Spearman correlation with a two-tailed
133 significance test to capture potentially non-linear dependencies. To ensure robustness and minimize sensitivity to arbitrary
134 cutoffs, this association analysis leveraged results derived from nine distinct DEG thresholds (as previously described) across
135 both JC/OC and PC metrics.

136 We observed pronounced positive correlations between sample size and study-wise convergence in Parkinson's substantia
137 nigra and peripheral blood, as well as in Crohn's ileal mucosa, for both AWmeta and REM (Fig. 3a–c). This reinforces the
138 principle that larger cohorts generally yield results that more closely approximate the consensus biological signal. Crucially,
139 at equivalent sample sizes, AWmeta consistently outperformed REM in convergence across all five disease tissues, where
140 performance gaps widened progressively with increasing sample size. To illustrate, using the adjusted DE list similarity metric
141 in Crohn's ileal mucosa, while AWmeta and REM exhibited comparable convergence scores (~0.38) at the same sample size
142 of 62, AWmeta's score surged to 0.77 at a sample size of 200—a 54% increase over REM's 0.50 (Fig. 3a), which demonstrates
143 AWmeta can reach much better convergence level under the same sample-size context. Notably, AWmeta attains comparable

144 convergence with considerably fewer samples relative to REM. To reach a convergence score of 0.2 in Parkinson's substantia
145 nigra, for instance, AWmeta necessitated 44% or 43% fewer samples than REM with JC/OC (15 versus 27; Fig. 3b) or PC
146 metric (20 versus 35; Fig. 3c). This marked improvement in sample efficiency translates directly into substantial reductions in
147 experimental cost and resource allocation.

148 We further hypothesized that DEG abundance would positively contribute to accurate meta-analytic estimates for gene
149 differential quantification and substantiated this premise through the observation of robust positive correlations between DEG
150 number and study-wise convergence across all five disease tissues (Fig. 3d–f), following the analogous procedure to the
151 above sample-size correlation analysis. For studies with similar DEG counts, AWmeta constantly yielded higher convergence
152 scores than REM, with performance disparity more pronounced as DEG abundance ascended, suggesting AWmeta possesses a
153 heightened sensitivity to the underlying biological signal embedded within scattered DEGs. For example, to arrive at a PC
154 metric-based convergence score of 0.4 in Crohn's peripheral blood, AWmeta required only 2,000 DEGs, whereas REM exacted
155 approximately 4,600—a 130% escalation—for equivalent resolution (Fig. 3f). This highlights AWmeta's capacity to achieve
156 robust convergence even from datasets with sparser DEG profiles, a practical advantage for experimental designs where DEG
157 discovery may be limited.

158 Collectively, these findings imply AWmeta can deliver reliable meta-analytic outcomes in less stringent experimental sce-
159 narios, such as studies involving milder treatments or designs with fewer replicates, which substantially mitigates experimental
160 complexity and cost, especially for ambitious large-scale research programs.

161 **AWmeta delivers remarkable stability and robustness in transcriptomic integration**

162 We sought to determine whether AWmeta's adaptively-weighted strategy confers superior stability and robustness to gene
163 differential meta-estimates against REM, and designed quantitative metrics to evaluate consistency over random splits and
164 resilience to systematic perturbations across the five disease tissues.

165 First, we assessed stability by quantifying the concordance of ranked gene differential lists derived from randomly halved
166 sample sets within each study, a process replicated across 100 iterations (Fig. 4a and "Stability and robustness assessment of
167 transcriptomic integration" in Methods). Across all five disease tissues, AWmeta exhibited markedly higher stability scores
168 relative to REM (Fig. 4b; $P < 10^{-4}$, one-tailed Welch's *t*-test), underscoring its enhanced consistency under data rationing.
169 The observation that median stability scores for both methods were below 0.7, is likely attributable to the inherently reduced
170 statistical power and study-wise convergence that accompanies halving the sample size (Fig. 3a).

171 We then challenged the robustness of each method against two distinct forms of perturbation: external interference,
172 simulated by the inclusion of a thematically unrelated study (Fig. 4c and "Stability and robustness assessment of transcriptomic
173 integration" in Methods), and internal fragility, evaluated through a systematic leave-one-study-out procedure (Fig. 4e and
174 "Stability and robustness assessment of transcriptomic integration" in Methods). Against external interference, AWmeta
175 displayed remarkable resilience with median robustness scores above 0.8 and established a significant performance margin over
176 REM across all tissues (Fig. 4d; $P < 10^{-4}, 10^{-2}$ or 0.05, one-tailed Mann-Whitney test). This capacity to resist discordant data
177 is a direct consequence of AWmeta's adaptive weighting scheme, which effectively minimizes the influence of outlier studies.
178 In internal robustness assessment, AWmeta again achieved significantly higher scores than REM in four of the five tissues
179 (Fig. 4f; $P < 0.05$, one-tailed Mann-Whitney test). The sole exception was Crohn's peripheral blood, where the small cohort of
180 only three studies constrained the median robustness scores to below 0.6 for both methods. Notably, in tissues comprising six
181 or more studies, AWmeta achieved exceptional median internal robustness scores around 0.9, demonstrating highly consistent
182 results even upon the exclusion of individual constituent studies.

183 These rigorous stress tests validate that AWmeta's adaptive weighting architecture endows the meta-analytic process with
184 significantly strengthened stability and robustness. This reinforcement ensures the derivation of more dependable biological
185 insights when integrating diverse and inherently heterogeneous transcriptomic datasets.

186 **AWmeta facilitates discovery of disease-relevant genes**

187 A pivotal determinant of a meta-analysis method's utility is its capacity to prioritize genes of genuine pathological importance.
188 To rigorously assess this, we quantified the biological relevance of gene rankings from AWmeta, REM, and the original studies
189 (as baselines) against authoritative Parkinson's and Crohn's disease-gene benchmarks—compiled from DisGeNET, MalaCards,
190 and an in-house curated genetic variation corpus—using a custom metric that integrates both statistical significance and effect
191 size magnitude, which provides an objective and threshold-agnostic evaluation of gene prioritization performance (Fig. 5a and
192 "Biological relevance assessment of gene differential quantification" section in Methods).

193 Prior to assessing performance, we first validated the coherence of our benchmark gene sets, with overlap magnitude
194 quantified using odds ratio (OR) and statistical significance determined by Fisher's exact test. Pairwise comparisons revealed
195 substantial overlaps among the three independent sources for both Parkinson's disease (e.g., DisGeNET versus MalaCards,
196 OR = 138.8, $P = 5.1 \times 10^{-15}$) and Crohn's disease (e.g., DisGeNET versus MalaCards, OR = 242.9, $P = 1.3 \times 10^{-27}$)
197 (Fig. 5b). This strong reciprocal consistency affirmed their utility for a reliable evaluation of biological relevance.

Our primary analysis revealed that AWmeta consistently generates more biologically meaningful gene rankings than REM and the baseline studies ($P < 10^{-4}, 10^{-3}, 10^{-2}$ or 0.05, Nemenyi post-hoc test; Fig. 5c–e). Specifically, when benchmarked against our genetic variant corpus, AWmeta achieved significantly higher relevance scores across all interrogated tissues (Fig. 5c). This superior performance extended to the DisGeNET benchmark in critical disease tissues, including Parkinson's substantia nigra and Crohn's peripheral blood and ileal mucosa (Fig. 5d). A similar advantage was observed using the MalaCards benchmark for Parkinson's substantia nigra and Crohn's ileal and colonic mucosa (Fig. 5e). Notably, AWmeta's superiority was particularly pronounced in the primary disease-affected tissues—Parkinson's substantia nigra and Crohn's ileal mucosa—where it surpassed baselines across all three independent benchmarks. Cumulatively, in 11 instances of the 15 tissue-benchmark comparisons (5 tissues \times 3 benchmarks), AWmeta's scores were significantly higher than those of both the baselines and REM. In stark contrast, REM failed to offer a significant improvement over baseline scores in 11 of 15 comparisons, underscoring its limited ability to distill new biological insights from existing data.

These results establish that AWmeta's gene prioritization is not merely a statistical refinement but a substantive improvement in biological fidelity. By more effectively elevating established disease-associated genes to the top of significance rankings, AWmeta provides a clearer and more accurate representation of the underlying pathology. This enhanced resolution positions AWmeta as a powerful discovery engine, capable of transforming heterogeneous transcriptomic datasets into a focused and mechanistically coherent view of disease processes.

AWmeta enables disease tissue-specific mechanism interpretation

We further implemented Gene Ontology (GO) enrichment to explore disease mechanism interpretation based on meta-analysis prioritized genes. To avoid arbitrariness, three thresholds (100, 300, and 500) were used to select the number of top integrated rank genes ("Biological relevance assessment of gene differential quantification" section in Methods). The enrichment ratio quantifies the degree to which GO terms are significantly enriched in relevant disease tissues:

$$\text{Enrichment ratio} = \frac{\text{Gene ratio}}{\text{Background ratio}} \quad (1)$$

where gene ratio is the proportion of genes annotated to a specific GO term within the top integrated rank genes, and background ratio represents the analogous fraction across a reference gene set. GO terms with higher enrichment ratios are more likely to be involved in a given disease tissue. For comparison, GO enrichments derived from original studies served as baselines.

Compared with REM and baselines, representative GO terms enriched in AWmeta-derived top integrated rank genes consistently exhibited the highest enrichment ratios across nearly all five disease tissues (Fig. 5f), demonstrating AWmeta's enhanced capacity for disease-relevant gene prioritization in tissue-specific contexts. In contrast, REM underperformed relative to some baselines (Fig. 5f), reflecting diminished biological relevance within its gene sets. For instance, biological processes related to synaptic organization and transmission ("synaptic transmission, dopaminergic", "regulation of synapse organization", and "distal axon") were significantly enriched in Parkinson's substantia nigra, consistent with their known involvement in Parkinson's pathogenesis^{25,26}. Likewise, "metal ion transmembrane transporter activity" and "regulation of membrane potential" were significantly enriched, highlighting their pivotal roles in Parkinson's substantia nigra-involved mechanisms^{27–29}. AWmeta achieved the highest enrichment for these GO terms, a trend robust across all thresholds. The enrichment ratios for AWmeta and some baselines monotonically decreased with more integrated rank genes included, indicating these term-related genes are concentrated at the very top of the ranked lists. Strikingly, REM-prioritized genes exhibited minimal or absent enrichment across all five representative GO terms, further underscoring its impaired capacity to capture contextual biological functions.

Given the well-established inflammatory pathogenesis of Parkinson's and Crohn's disease in non-hematopoietic tissues^{30,31}, we hypothesized that blood-derived gene signatures would reflect systemic immune dysregulation and vascular barrier impairment at disease-relevant interfaces: Parkinson's blood-brain barrier and Crohn's intestinal vasculature. Peripheral blood analyses revealed significant enrichment of immune-related GO terms in Parkinson's disease, including "MHC protein complex"³², "antigen binding"³³, and "immunoglobulin complex". The circulatory specificity was further evidenced by "humoral immune response mediated by circulating immunoglobulin". Similarly, in Crohn's peripheral blood, neutrophil-related GO terms ("neutrophil degranulation", "neutrophil activation involved in immune response", "neutrophil mediated immunity", and "neutrophil activation") indicated the involvement of immune-inflammatory processes³⁴. Furthermore, significant Parkinson's "complement activation" and Crohn's "blood coagulation" provided disease-specific vascular insights. Aberrant complement system activity may imply blood-brain barrier disruption in Parkinson's patients^{35,36}, whereas increased venous thromboembolism risk in Crohn's patients due to abnormal coagulation³⁷ indicates intestinal vascular barrier impairment³⁸.

The ileal and colonic mucosa constitute primary pathological sites in Crohn's disease³¹, where collagen plays a key role in extracellular matrix remodeling³⁹, evidenced by the significant "collagen catabolic process". Gut microbiota dysbiosis, reflected by GO terms "antimicrobial humoral response" and "response to lipopolysaccharide", further aligned with Crohn's pathogenesis^{40,41}. While Crohn's ileal and colonic mucosa share multifaceted similarities, they displayed two key distinctions:

249 complement activation and digestion. Although both mucosal tissues showed complement activation, its enrichment ratios were
250 2-4 times higher in ileal versus colonic mucosa, supported by immunofluorescence staining and single-cell transcriptomics
251 indicating more active complement activation in ileal mucosa^{42,43}. It has been generally acknowledged the ileal mucosa
252 uniquely mediates hydrolase-driven enzymatic digestion, whereas the colonic mucosa plays no substantive role in chemical
253 digestion⁴⁴. This functional dichotomy was corroborated by the enrichments of the "digestion" GO term: AWmeta specifically
254 detected "digestion" within top 100 ileal mucosa genes (highest enrichment), whereas REM and baselines showed delayed
255 identification (top 300/500 genes; lower enrichment); conversely, AWmeta consistently excluded "digestion" from colonic
256 mucosa enrichments, in contrast to sporadic false positives by these counterparts. These functional stratifications demonstrate
257 AWmeta's enhanced biological fidelity in resolving disease tissue-contextual gene functions.

258 Discussion

259 Transcriptomic meta-analysis is pivotal for distilling robust biological insights from heterogeneous gene expression studies; yet,
260 existing frameworks remain confined to either *P*-value combination or effect-size integration, imposing a trade-off between
261 statistical sensitivity and quantitative fidelity. A unified strategy that seamlessly integrates both paradigms—capitalizing on
262 their complementary strengths while circumventing their individual limitations—has therefore been a long-standing, unmet
263 imperative.

264 AWmeta represents the first successful integration of *P*-value and effect-size aggregation methodologies in transcriptomic
265 meta-analysis. The core innovation—a cross-module information transfer where optimized weights from *P*-value calculations
266 directly enhance effect size estimation—effectively addresses between-study heterogeneity while maximizing consistent
267 biological signal extraction. Indeed, the substantial variability often observed between studies, visually apparent in metrics like
268 gene-wise convergence (Fig. 2b–f with per-study skewed distributions), highlights the prevalence of such heterogeneity and
269 strongly supports the usage of random-effects-like frameworks such as AWmeta and REM over simpler fixed-effects models⁴⁵.
270 In our comprehensive evaluation across 35 datasets from Parkinson's and Crohn's disease, AWmeta demonstrated superior
271 high-fidelity DEG detection that remained robust under substantial experimental noise (Fig. 1c,g–i and Extended Data Fig. 2–5).
272 This enhanced discrimination capacity enabled identification of subtle yet biologically meaningful expression changes that
273 conventional methods frequently miss, substantially improving the reliability and reproducibility of transcriptomic discoveries.

274 Our convergence metrics revealed AWmeta's practical advantages in approximating theoretical true values at both gene and
275 study levels. It's noteworthy that in our gene-wise convergence assessments, some original studies occasionally outperformed
276 standard REM, even without larger sample sizes (Fig. 2b–f and Extended Data Fig. 6). While not conclusive, this hints that
277 inherent study quality or specific experimental contexts might significantly influence reliability, perhaps as much as sample
278 size itself. We also observed a tendency for these well-performing studies to utilize RNA-seq technology. These observations
279 underscore the complexity of integrating diverse datasets and highlight the benefit of AWmeta's adaptive capability which
280 weights studies based on informational content rather than relying solely on metrics like sample size. AWmeta achieved
281 equivalent study-wise convergence with significantly fewer samples and DEGs than conventional methods—a critical advantage
282 in resource-constrained research environments that can substantially reduce experimental costs and researcher workload.

283 The superior biological relevance of AWmeta's findings was rigorously established through two orthogonal and comple-
284 mentary assessment paradigms: (1) Using authoritative disease-specific gene sets from DisGeNET, MalaCards, and in-house
285 genetic variant corpus, AWmeta demonstrated significantly enhanced biological meaningfulness. In 11 of 15 tissue-benchmark
286 combinations, AWmeta outperformed both REM and original studies in biological relevance scoring (Fig. 5c–e). This consistent
287 advantage provides researchers with more accurate representations of core disease pathways and creates unprecedented oppor-
288 tunities for discovering novel pathophysiological relationships that remain obscured in conventional analyses. (2) Longitudinal
289 tracking of GO term enrichment across gene rank thresholds revealed AWmeta's unique capacity to concentrate functionally
290 critical genes within leading ranks. While terms of secondary importance (e.g., "MHC protein complex", "blood coagulation")
291 showed delayed enrichment beyond top 300 ranks across all methods (Fig. 5f), pathologically central functions exhibited
292 exclusive early enrichment in AWmeta. Crucially, terms like "digestion" in Crohn's ileal mucosa reached peak enrichment
293 exclusively within AWmeta's top 100 genes (Fig. 5f), with no detection at expanded thresholds; REM failed to detect this
294 pivotal function at both top 100 and 300 thresholds, achieving only marginal detection at top 500 (Fig. 5f)—demonstrating its
295 fundamental limitations in biological resolution. This enrichment trajectory analysis establishes a dual-purpose paradigm for
296 quantitatively evaluating gene prioritization performance and objectively stratifying biological mechanisms by pathological
297 centrality. Together, these orthogonal validation strategies—leveraging curated knowledgebases and temporal enrichment
298 dynamics—provide compelling evidence that AWmeta uniquely reconciles statistical rigor with biological fidelity, transforming
299 heterogeneous transcriptomic data into precisely stratified mechanistic insights.

300 While AWmeta represents a significant advance, several aspects warrant consideration for broader application. The method's
301 computational complexity, though tractable for typical multi-study analyses, may require optimization for emerging consortia-
302 level datasets exceeding 100 studies. Performance is also intrinsically linked to input data quality; while adaptive weighting

303 mitigates variable study quality (Fig. 2b–f and Extended Data Fig. 6), unaddressed technical artifacts (e.g., severe batch effects)
304 could subtly influence results. Furthermore, the current framework focuses on gene-level differential quantification; extension
305 to isoform-resolution or splicing analysis would require adaptation to handle increased dimensionality. Finally, scenarios
306 involving extreme, systematic confounding across studies (e.g., irreconcilable patient stratification) remain challenging—a
307 limitation pervasive among meta-analytic methods.

308 These considerations highlight clear pathways for AWmeta’s evolution, complementary to its core strengths. Algorithmic
309 refinements such as distributed computing could enhance scalability for ultra-large-scale integrations. Furthermore, incorporating
310 tissue-specific molecular networks or multi-omic layers (e.g., epigenomics, proteomics) would refine biological inference
311 beyond expression-centric views. Notably, coupling AWmeta with pharmacological databases holds significant promise for
312 *in silico* drug target prioritization and biomarker discovery. The framework also uniquely empowers researchers to integrate
313 limited-scale local datasets with public repositories, democratizing access to robust meta-analysis and amplifying statistical
314 power for domain investigations.

315 Crucially, the present AWmeta implementation already delivers immediate, high-impact utility. It establishes a robust
316 new standard for extracting reliable biological signals from complex, heterogeneous transcriptomic data—overcoming a
317 fundamental methodological dichotomy that has long constrained the field. By synergistically combining *P*-value and effect
318 size paradigms, AWmeta enhances reproducibility and biological interpretability, directly accelerating the translation of
319 transcriptomic discoveries into clinical insights and biotechnological applications. This methodological leap provides an
320 integral tool for navigating the growing complexity of precision transcriptomic integration in biomedical research.

321 **Methods**

322 **Overview of the AWmeta framework**

323 The transformative potential of AWmeta stems from its adaptively weighting scheme, which strategically prioritizes the most
 324 informative studies while robustly mitigating noise and outliers to yield biologically coherent, high-fidelity meta-analytic
 325 estimates. This framework performs gene-by-gene meta-analysis of heterogeneous transcriptomic studies by integrating
 326 per-study gene summary statistics (Fig. 1a). For each gene, input from each study in the valid set (S_{gene}) comprises: (1) a
 327 P -value (P_i), (2) a log₂-based fold change (FC_i), and (3) its corresponding within-study variance (Var_i), all derived from the
 328 original gene differential quantification analyses. AWmeta consists of two sequential modules: *AW-Fisher* for adaptive P -value
 329 aggregation and *AW-REM* for adaptive effect-size integration. Studies absent from S_{gene} (e.g., Study₂ with missing P_2 , FC_2 , or
 330 Var_2) are excluded a priori.

331 ***AW-Fisher module (adaptive P-value integration)***

332 Within this module, each gene's meta P -value is obtained by selecting an optimal subset of S_{gene} that minimizes a weighted
 333 Fisher's statistic-derived combined P -value⁹. Let $N' = |S_{gene}|$ be the number of studies reporting P -values for the gene,
 334 with $S'_{gene} = \{1, \dots, N'\}$ enumerating the study indices, and denote their P -values by $\vec{\mathbf{P}} = (P_1, \dots, P_i)_{i \in S'_{gene}} \in (0, 1)^{N'}$. The
 335 corresponding binary weight vector, $\vec{\mathbf{w}} = (w_1, \dots, w_i)_{i \in S'_{gene}} \in \{0, 1\}^{N'}$, indicates inclusion ($w_i = 1$) or exclusion ($w_i = 0$) of
 336 Study_i $\in S_{gene}$ in the final subset. The AW-Fisher statistic is defined as:

$$T(\vec{\mathbf{P}}; \vec{\mathbf{w}}) = -2 \sum_{i \in S'_{gene}} w_i \ln P_i \quad (2)$$

337 The significance level of $T(\vec{\mathbf{P}}; \vec{\mathbf{w}})$ under the null hypothesis is calculated using the chi-squared distribution:

$$L(T(\vec{\mathbf{P}}; \vec{\mathbf{w}})) = 1 - F_{\chi_d^2(\vec{\mathbf{w}})}(T(\vec{\mathbf{P}}; \vec{\mathbf{w}})) \quad (3)$$

338 where the degrees of freedom are $d(\vec{\mathbf{w}}) = 2 \sum_{i \in S'_{gene}} w_i$, and $F_{\chi_d^2}(\cdot)$ is the cumulative distribution function of the chi-squared
 339 distribution with d degrees of freedom.

340 The meta P -value, $s(\vec{\mathbf{P}})$, is the minimum significance level obtained by optimizing the weight vector over the studies in
 341 S_{gene} :

$$s(\vec{\mathbf{P}}) = \min_{\vec{\mathbf{w}}} L(T(\vec{\mathbf{P}}; \vec{\mathbf{w}})) \quad (4)$$

342 The optimal weight vector $\hat{\mathbf{w}}$ that achieves this minimum is determined by:

$$\hat{\mathbf{w}} = w(\vec{\mathbf{P}}) = \operatorname{argmin}_{\vec{\mathbf{w}}} L(T(\vec{\mathbf{P}}; \vec{\mathbf{w}})) = (\hat{w}_1, \dots, \hat{w}_i)_{i \in S'_{gene}} \quad (5)$$

343 This optimal weight vector $\hat{\mathbf{w}}$, containing binary weights for each study in S_{gene} , is passed to the following AW-REM module.

344 ***AW-REM module (adaptive effect-size integration)***

345 This module calculates the meta effect size (log₂FC) using an adaptively-weighted REM. It leverages the log₂FC (FC_i) and
 346 within-study variance (Var_i) from studies in S_{gene} , modulated by the optimal binary weights $\hat{\mathbf{w}}$ derived from the AW-Fisher
 347 module for those same studies. The contribution weight for Study_i $\in S_{gene}$ in AW-REM is defined as:

$$W_i = \frac{\hat{w}_i}{Var_i + T^2} \quad (6)$$

348 where \hat{w}_i is the binary weight (0 or 1) for Study_i $\in S_{gene}$ from Eq. 5. Var_i is the within-study variance for the gene in Study_i,
 349 and T^2 represents the between-study variance, estimated using restricted maximum likelihood (REML) method⁴⁶. W_i is zero
 350 whenever $\hat{w}_i = 0$, thus automatically omitting studies not selected by AW-Fisher module.

351 The final meta fold change, denoted \mathbf{M} , is computed as an adaptively calibrated average of the study-wise effect sizes:

$$\mathbf{M} = \frac{\sum_{i \in S'_{gene}} W_i FC_i}{\sum_{i \in S'_{gene}} W_i} \quad (7)$$

352 This formulation delivers a consensus fold-change estimate both statistically rigorous and quantitatively faithful to the most
 353 informative subsets of heterogeneous studies.

354 **Transcriptomic datasets**

355 To proof-of-concept the AWmeta framework, we compiled 35 publicly available human transcriptomic datasets for Parkinson's
356 and Crohn's disease from the Gene Expression Omnibus (GEO)⁴⁷, Sequence Read Archive (SRA)⁴⁸, and ArrayExpress⁴⁹.
357 These datasets, encompassing both microarray and RNA-sequencing (RNA-seq) platforms, included samples derived from
358 Parkinson's substantia nigra^{50–57} and peripheral blood^{53,58–65}, Crohn's peripheral blood^{66–68}, ileal mucosa^{69–74} and colonic
359 mucosa^{73–79}. A complete list of the datasets, detailing data accession IDs, sequencing platform identifiers, dataset and tissue
360 sources, and patient and control sample sizes, is provided in Extended Data Fig. 1.

361 **Transcriptomic data preprocessing**

362 Due to the inclusion of datasets generated on different platforms, specific preprocessing pipelines were applied separately to
363 microarray and RNA-seq data.

364 **Microarray data processing**

365 To ensure accurate and up-to-date probe annotations, microarray probe identifiers were mapped to Entrez Gene IDs using
366 information retrieved from GEO SOFT files, platform-specific Bioconductor annotation packages, and the AnnoProbe R
367 package. For genes represented by multiple probes, we retained the probe with the largest interquartile range (IQR) of intensities
368 across samples to maximize biological informativeness^{21,80}. Subsequently, the limma R package⁸¹ was utilized for microarray
369 data preprocessing, normalization, and differential gene identification. Gene differential quantification (case versus control)
370 within each study was determined via empirical Bayes moderated *t*-statistics, yielding per-gene P_i , FC_i , and Var_i .

371 **RNA-seq data processing**

372 RNA-seq data were processed through an automated snakemake workflow⁸². Raw sequencing reads were processed with
373 Trimmomatic⁸³ to remove adapter sequences and low-quality bases. Following best practice recommendations⁸⁴, the cleaned
374 reads were aligned to the human reference genome (GRCh38 assembly) using HISAT2⁸⁵. Gene-level read counts were
375 quantified from the aligned reads using featureCounts⁸⁶. Finally, we performed gene differential quantification with DESeq2⁸⁷,
376 producing per-gene P_i , FC_i , and Var_i for each study.

377 **Transcriptomic meta-analysis evaluation metrics**

378 To impartially evaluate AWmeta's performance advances, we conducted a multi-dimensional comparison against the current
379 gold-standard REM method^{6,21,22} across the following critical analytical domains: (i) DEG detection capability, (ii) DEG
380 discrimination, (iii) gene- and study-wise gene differential quantification convergence, (iv) stability and robustness, and (v)
381 biological relevance. Both methods operated on matching inputs and identical gene sets, ensuring an equitable performance
382 assessment.

383 **DEG detection capability evaluation**

384 DEG detection capability is defined as the gene count satisfying pre-defined thresholds for both corrected statistical significance
385 P -value (FDR) and fold change magnitude ($\log_2 FC$) (Fig. 1b). To assess the stability and reliability of this capability, we
386 implemented a bootstrap resampling strategy with 100 iterations. In each iteration, we created bootstrapped datasets by
387 randomly sampling with replacement from the original case and control groups while maintaining the original sample sizes,
388 followed by meta-analysis. The resulting DEG counts formed a distribution for statistical comparison with one-tailed Welch's
389 *t*-test.

390 **DEG discrimination evaluation using semi-synthetic simulation strategy**

391 To evaluate the ability to discriminate between DEGs and non-DEGs, particularly considering potential false positives arising
392 from higher detection sensitivity, we adopted an evaluation metric based on semi-synthetic simulated data, inspired by Li and
393 colleagues²³. This approach consisted of benchmark dataset generation and evaluation using datasets with simulated noise
394 (Fig. 1d–f) and for each tissue context:

- 395 1. Identify the intersection of DEGs and non-DEGs called by both AWmeta and REM under predefined screening thresholds
396 (Fig. 1d).
- 397 2. Randomly sample half of the intersected DEGs to form an unbiased positive benchmark; sample an equal-sized negative
398 benchmark from the intersected non-DEGs (Fig. 1d).
- 399 3. Construct semi-synthetic datasets by permuting case/control labels within a subset of original studies (e.g., Study₁ and
400 Study₃; Fig. 1e). Label permutation removes true signal from those studies.
- 401 4. Apply AWmeta and REM to the combined set of original and label-permuted studies; compute the AUROC and AUPRC
402 over the previously defined positive and negative benchmark genes (Fig. 1e).

403 5. Repeat Steps 3 and 4 for 100 times to obtain distributions of AUROC and AUPRC, summarizing performance under
 404 minimum-, median-, and maximum-permuted scenarios (Fig. 1f), which ensures the stability and reliability of our
 405 assessment. Statistical significance between AWmeta and REM was tested via one-tailed Mann–Whitney test.

406 **Gene-wise convergence assessment for gene differential quantification**

407 To assess per-gene differential quantification agreement between meta-analysis (FC_{meta}) and original constituent studies (FC_i),
 408 we computed a MAD-like gene-wise convergence score (Fig. 2a). For each gene \mathcal{G} :

$$C_{\mathcal{G}meta} = \frac{1}{|S_{gene}|} \sum_{i \in S'_{gene}} |FC_{meta} - FC_i| \quad (8)$$

409 where S_{gene} and S'_{gene} denote the valid study set and corresponding indices for the gene (defined in "Overview of the AWmeta
 410 framework" section), $|S_{gene}|$ the cardinality of the set S_{gene} , $FC_{meta} = \mathbf{M}$ from Eq. 7 and FC_i is the study-exclusive log₂-based
 411 fold change. A lower $C_{\mathcal{G}meta}$ implies better agreement between the meta-analysis and original study estimates within S_{gene} . For
 412 baseline comparison, we also computed, for each original Study_j $\in S_{gene}$, a gene-wise convergence score:

$$C_{\mathcal{G}j} = \frac{1}{|S_{gene}|} \sum_{i \in S'_{gene}} |FC_j - FC_i| \quad (9)$$

413 which represents the MAD of Study_j's fold change from all other contributing studies. This internal consistency benchmark
 414 enables direct contrast of AWmeta's and REM's convergence performance against the inherent agreement among the original
 415 datasets. All comparisons used one-tailed Mann–Whitney test against AWmeta.

416 **Study-wise convergence assessment for gene differential quantification**

417 To rigorously evaluate the consistency between gene lists derived from meta-analysis methods and those from the original
 418 studies, we employed three complementary approaches. For all metrics, higher scores indicate superior study-level convergence.

419 1. **Adjusted rankED genE (DE) list similarity:** Our first approach quantifies concordance using a rank-sensitive similarity
 420 metric that is critically weighted towards top-ranked genes (Fig. 2g and Extended Data Fig. 7). To construct robustly
 421 ordered gene lists (G_{meta} for the meta-analysis; G_i for Study_i), we first devised a composite rank for each gene by
 422 multiplying its *P*-value rank (ascending) with its $|\log_2 FCI|$ rank (descending), thereby integrating statistical significance
 423 and effect size.

424 The weighted similarity $S(G_{meta}, G_i)$ between the meta-analysis and each original study gene lists (containing N genes)
 425 was computed using a non-linear weighting scheme⁸⁸, which emphasizes the top-ranked gene concordance:

$$S(G_{meta}, G_i) = \sum_{n=1}^N e^{-\alpha n} O_n(G_{meta}, G_i) \quad (10)$$

426 where $O_n(G_{meta}, G_i)$ is the number of common genes in the top n positions and α is a weighting exponent (0.001). This
 427 score was then normalized to the interval $[-1, 1]$ ²² yielding the adjusted similarity:

$$S_{adj}(G_{meta}, G_i) = \frac{S(G_{meta}, G_i) - E_{null}(S(G_{meta}, G_i))}{\max(S(G_{meta}, G_i)) - E_{null}(S(G_{meta}, G_i))} \quad (11)$$

428 where $E_{null}(S(G_{meta}, G_i)) = \sum_{n=1}^N \frac{n^2}{N} e^{-\alpha n}$ and $\max(S(G_{meta}, G_i)) = \sum_{n=1}^N n e^{-\alpha n}$ are the expected and maximum scores
 429 under a null hypothesis of random gene lists.

430 2. **Set-based overlap similarity:** To circumvent the limitations of the above rank-dependent approach, which is sensitive to
 431 gene ranking variations while potentially overlooking consistent differential expression patterns, we assessed study-wise
 432 convergence using a set-based overlap metric that exclusively evaluates binary DEG classification concordance (Fig. 2h,i).
 433 Here, DEG sets were determined for both the meta-analysis (Set_{meta}) and individual studies (Set_i) using predefined
 434 statistical thresholds, thereby focusing analytical power on reproducible differential expression status irrespective of
 435 positional gene rankings.

436 We calculated two complementary metrics: JC ($JC_i = |Set_{meta} \cap Set_i| / |Set_{meta} \cup Set_i|$) and OC ($OC_i = |Set_{meta} \cap$
 437 $Set_i| / \min(|Set_{meta}|, |Set_i|)$). The convergence metric for the meta-analysis relative to Study_i was the arithmetic mean
 438 ($JC_i + OC_i$)/2.

439 3. **Phi coefficient similarity:** Finally, we measured the association between DEG classifications using phi coefficient²⁴ (ϕ)
 440 (Fig. 2h,j). This approach considers the extreme case where shared DEGs or non-DEGs between two gene sets might be
 441 randomly generated.

442 For each comparison between the meta-analysis and an original Study_i, we constructed a 2×2 contingency table
 443 categorizing all genes as DEG or non-DEG in both datasets and the phi coefficient (ϕ) was then calculated as:

$$\phi_i = \frac{n_{11}n_{22} - n_{12}n_{21}}{\sqrt{n_1.n_2.n_{.1}n_{.2}}} \quad (12)$$

444 where n_{11} represents DEGs, n_{22} non-DEGs in both datasets, and n_{12} and n_{21} represent exclusively-classified DEGs for
 445 the binary datasets. The row and column sums are denoted by n_1 , n_2 , $n_{.1}$, and $n_{.2}$.

446 To establish a performance baseline, we computed all three convergence metrics for every pairwise combination of the
 447 original studies. Overall study-wise convergence differences among AWmeta, REM and baselines were tested by Kruskal–Wallis
 448 test, followed by Nemenyi post-hoc test for pairwise comparisons.

449 For the set-based and ϕ metrics, which rely on binary DEG and non-DEG classification, we note that these outcomes are
 450 mutually exclusive and complementary, and therefore report the results derived from the DEG sets for clarity and conciseness.

451 **Stability and robustness assessment of transcriptomic integration**

452 To demonstrate AWmeta’s resilience, we evaluated both stability—against stochastic sampling—and robustness—against dataset
 453 perturbations—using the adjusted DE list similarity (“Study-wise convergence assessment for gene differential quantification”
 454 section and Extended Data Fig. 7).

455 1. **Within-study subsampling stability:** For each original cohort, we randomly partitioned case and control samples of
 456 every study into two equal subcohorts, yielding paired “half-study” datasets. Each half-study set underwent independent
 457 DEG analysis and subsequent meta-analysis. The similarity between the resulting ordered gene lists was computed
 458 over 100 bootstrap replicates, quantifying stability under within-study sampling (Fig. 4a). AWmeta and REM stability
 459 distributions were compared via one-tailed Welch’s *t*-test.

460 2. **External robustness:** We assessed resilience to new data by sequentially incorporating one independent external study
 461 (from a held-out pool) into the original meta-analysis (Fig. 4c). For each addition, we performed meta-analysis pre- and
 462 post-inclusion, then computed adjusted DE list similarity between resulting ordered gene lists, measuring the impact of
 463 disparate external data (AWmeta versus REM, one-tailed Mann–Whitney test).

464 3. **Internal robustness:** We evaluated sensitivity to study omission by performing leave-one-study-out analyses (Fig. 4e):
 465 each original study was removed in turn, and meta-analyses were rerun on the reduced datasets. The similarity between
 466 each leave-one-study-out and the full-cohort ranked gene lists, across all iterations, quantified internal robustness
 467 (AWmeta versus REM, one-tailed Mann–Whitney test).

468 **Biological relevance assessment of gene differential quantification**

469 To quantify disease-context relevance of gene differential quantification, we assembled benchmark gene sets for Parkinson’s and
 470 Crohn’s disease from three sources: (1) DisGeNET⁸⁹ with gene-disease association (GDA) score > 0.2^{90,91}, (2) MalaCards⁹²,
 471 and (3) our in-house curated disease-related genetic variation corpus (will release soon). For reference comparisons, original
 472 study-derived biological relevance results serve as baselines.

473 For each method (AWmeta, REM or baselines), all analyzed genes were ranked twice—(i) by descending $|\log_2\text{FC}|$, (ii) by
 474 ascending *P*-value—then each benchmark gene’s ranks were multiplied:

$$\text{Integrated Rank} = \text{Rank}_{|\log_2\text{FC}|} \times \text{Rank}_{P\text{-value}} \quad (13)$$

475 Benchmark genes were then re-ranked according to this Integrated Rank (ascending) to obtain $\text{Rank}_{\text{Integrated Rank}}$. The Biological
 476 Relevance score was calculated for each benchmark gene as:

$$\text{Biological Relevance} = 1 - \frac{\text{Rank}_{\text{Integrated Rank}}}{N} \quad (14)$$

477 where N is the size of gene list from AWmeta, REM or baselines. Higher scores reflect greater biological relevance, signifying
 478 that benchmark genes attain superior rankings through combining statistical significance and fold change (Fig. 5a). This
 479 rank-based score accounts for gene list size heterogeneity and avoids arbitrary DEG thresholds. We compared biological
 480 relevance distributions from AWmeta, REM and baselines using Kruskal–Wallis and Nemenyi post-hoc test.

481 Data availability

482 All transcriptomic datasets used in this study are publicly available via GEO, SRA, and ArrayExpress. Parkinson's disease data
483 include substantia nigra (GEO accessions: GSE114517, GSE8397, GSE20163, GSE20164, GSE20292, GSE7621,
484 GSE49036, GSE42966, GSE43490, GSE26927, GSE54282) and peripheral blood (GEO accessions: GSE57475,
485 GSE54536, GSE34287, GSE99039, GSE72267, GSE6613, GSE18838, GSE165082). Crohn's disease datasets include
486 peripheral blood (GEO accessions: GSE119600, GSE112057, GSE94648), ileal mucosa (GEO accessions: GSE102133,
487 GSE75214, GSE16879, GSE68570, GSE101794, GSE57945), and colonic mucosa (GEO accessions: GSE75214,
488 GSE16879, GSE36807, GSE4183, GSE9686, GSE66207; ArrayExpress accession: E-MTAB-184). Benchmark gene
489 sets for both diseases were retrieved from DisGeNET (<https://www.disgenet.com/>) and MalaCards (<https://www.malacards.org/>).

491 Code availability

492 AWmeta is available on GitHub at <https://github.com/YanshiHu/AWmeta>.

493 References

- 494 1. Stark, R., Grzelak, M. & Hadfield, J. Rna sequencing: the teenage years. *Nat. Rev. Genet.* **20**, 631–656 (2019).
- 495 2. Shorten, A. & Shorten, B. What is meta-analysis? *Evid. Based Nurs.* **16**, 3–4 (2013).
- 496 3. Piras, I. S. *et al.* Peripheral biomarkers in schizophrenia: a meta-analysis of microarray gene expression datasets. *Int. J. Neuropsychopharmacol.* **22**, 186–193 (2019).
- 497 4. Zhong, G., Bolitho, S., Grunstein, R., Naismith, S. L. & Lewis, S. J. G. The relationship between thermoregulation and
498 rem sleep behaviour disorder in parkinson's disease. *PLoS One* **8**, e72661 (2013).
- 500 5. Cho, H. *et al.* Meta-analysis method for discovering reliable biomarkers by integrating statistical and biological approaches:
501 An application to liver toxicity. *Biochem. Biophys. Res. Commun.* **471**, 274–281 (2016).
- 502 6. Makinde, F. L. *et al.* Reviewing and assessing existing meta-analysis models and tools. *Briefings Bioinforma.* **22**, bbab324
503 (2021).
- 504 7. Fisher, R. A. Statistical methods for research workers. In *Breakthroughs in statistics: Methodology and distribution*, 66–70
505 (Springer, 1970).
- 506 8. Stouffer, S. A. A study of attitudes. *Sci. Am.* **180**, 11–15 (1949).
- 507 9. Li, J. & Tseng, G. C. An adaptively weighted statistic for detecting differential gene expression when combining multiple
508 transcriptomic studies. *Annals Appl. Stat.* **5**, 994–1019 (2011).
- 509 10. Wang, X. *et al.* Comparing methods for performing trans-ethnic meta-analysis of genome-wide association studies. *Hum.
510 molecular genetics* **22**, 2303–2311 (2013).
- 511 11. Toro-Domínguez, D. *et al.* A survey of gene expression meta-analysis: methods and applications. *Briefings Bioinforma.*
512 **22**, 1694–1705 (2021).
- 513 12. Romano, S. *et al.* Machine learning-based meta-analysis reveals gut microbiome alterations associated with parkinson's
514 disease. *Nat. Commun.* **16**, 1–17 (2025).
- 515 13. Yang, J., Liu, Q. & Shyr, Y. A large-scale meta-analysis reveals positive feedback between macrophages and t cells that
516 sensitizes tumors to immunotherapy. *Cancer research* **84**, 626–638 (2024).
- 517 14. Powell, N. R. *et al.* Clinically important alterations in pharmacogene expression in histologically severe nonalcoholic fatty
518 liver disease. *Nat. Commun.* **14**, 1474 (2023).
- 519 15. Langan, D. Assessing heterogeneity in random-effects meta-analysis. In *Meta-research: methods and protocols*, 67–89
520 (Springer, 2021).
- 521 16. Breitling, R., Armengaud, P., Amtmann, A. & Herzyk, P. Rank products: a simple, yet powerful, new method to detect
522 differentially regulated genes in replicated microarray experiments. *FEBS Lett.* **573**, 83–92 (2004).
- 523 17. Del Carratore, F. *et al.* Rankprod 2.0: a refactored bioconductor package for detecting differentially expressed features in
524 molecular profiling datasets. *Bioinformatics* **33**, 2774–2775 (2017).
- 525 18. Tseng, G. C., Ghosh, D. & Feingold, E. Comprehensive literature review and statistical considerations for microarray
526 meta-analysis. *Nucleic acids research* **40**, 3785–3799 (2012).

- 527 19. Aguzzoli Heberle, B. *et al.* Systematic review and meta-analysis of bulk rnaseq studies in human alzheimer's disease brain
528 tissue. *Alzheimer's & Dementia* **21**, e70025 (2025).
- 529 20. Stogiannis, D., Siannis, F. & Androulakis, E. Heterogeneity in meta-analysis: a comprehensive overview. *The Int. J.*
530 *Biostat.* **20**, 169–199 (2024).
- 531 21. Ma, T. *et al.* Metaomics: analysis pipeline and browser-based software suite for transcriptomic meta-analysis. *Bioinformatics*
532 **35**, 1597–1599 (2019).
- 533 22. Chang, L.-C., Lin, H.-M., Sibille, E. & Tseng, G. C. Meta-analysis methods for combining multiple expression profiles:
534 comparisons, statistical characterization and an application guideline. *BMC Bioinforma.* **14**, 368 (2013).
- 535 23. Li, Y., Ge, X., Peng, F., Li, W. & Li, J. J. Exaggerated false positives by popular differential expression methods when
536 analyzing human population samples. *Genome Biol.* **23**, 79 (2022).
- 537 24. Akoglu, H. User's guide to correlation coefficients. *Turkish J. Emerg. Medicine* **18**, 91–93 (2018).
- 538 25. Hu, Y., Pan, Z., Hu, Y., Zhang, L. & Wang, J. Network and pathway-based analyses of genes associated with parkinson's
539 disease. *Mol. neurobiology* **54**, 4452–4465 (2017).
- 540 26. Burke, R. E. & O'Malley, K. Axon degeneration in parkinson's disease. *Exp. neurology* **246**, 72–83 (2013).
- 541 27. Chen, L. *et al.* Homeostasis and metabolism of iron and other metal ions in neurodegenerative diseases. *Signal Transduct.*
542 *Target. Ther.* **10**, 31 (2025).
- 543 28. Bjorklund, G. *et al.* Metals and parkinson's disease: mechanisms and biochemical processes. *Curr. Medicinal Chem.* **25**,
544 2198–2214 (2018).
- 545 29. Ma, K. Y., Fokkens, M. R., Reggiori, F., Mari, M. & Verbeek, D. S. Parkinson's disease-associated vps35 mutant reduces
546 mitochondrial membrane potential and impairs pink1/parkin-mediated mitophagy. *Transl. neurodegeneration* **10**, 1–17
547 (2021).
- 548 30. Poewe, W. *et al.* Parkinson disease. *Nat. reviews Dis. primers* **3**, 1–21 (2017).
- 549 31. Roda, G. *et al.* Crohn's disease. *Nat. Rev. Dis. Primers* **6**, 22 (2020).
- 550 32. Gu, R. *et al.* The major histocompatibility complex participates in parkinson's disease. *Pharmacol. Res.* 107168 (2024).
- 551 33. Tan, E.-K. *et al.* Parkinson disease and the immune system—associations, mechanisms and therapeutics. *Nat. Rev. Neurol.*
552 **16**, 303–318 (2020).
- 553 34. Danne, C., Skerniskyte, J., Marteyn, B. & Sokol, H. Neutrophils: from ibd to the gut microbiota. *Nat. Rev. Gastroenterol.*
554 & Hepatol.
- 555 35. Nimmo, J. *et al.* The complement system in neurodegenerative diseases. *Clin. Sci.* **138**, 387–412 (2024).
- 556 36. Khosousi, S. *et al.* Complement system changes in blood in parkinson's disease and progressive supranuclear
557 palsy/corticobasal syndrome. *Park. & Relat. Disord.* **108**, 105313 (2023).
- 558 37. Rogler, G., Singh, A., Kavanaugh, A. & Rubin, D. T. Extraintestinal manifestations of inflammatory bowel disease: current
559 concepts, treatment, and implications for disease management. *Gastroenterology* **161**, 1118–1132 (2021).
- 560 38. Stadnicki, A. & Stadnicka, I. Venous and arterial thromboembolism in patients with inflammatory bowel diseases. *World*
561 *journal gastroenterology* **27**, 6757 (2021).
- 562 39. Mortensen, J. *et al.* The intestinal tissue homeostasis—the role of extracellular matrix remodeling in inflammatory bowel
563 disease. *Expert. review gastroenterology & hepatology* **13**, 977–993 (2019).
- 564 40. Caruso, R., Lo, B. C. & Núñez, G. Host–microbiota interactions in inflammatory bowel disease. *Nat. Rev. Immunol.* **20**,
565 411–426 (2020).
- 566 41. Candelli, M. *et al.* Interaction between lipopolysaccharide and gut microbiota in inflammatory bowel diseases. *Int. journal*
567 *molecular sciences* **22**, 6242 (2021).
- 568 42. Halstensen, T., Mollnes, T., Garred, P., Fausa, O. & Brandtzaeg, P. Surface epithelium related activation of complement
569 differs in crohn's disease and ulcerative colitis. *Gut* **33**, 902–908 (1992).
- 570 43. Kong, L. *et al.* The landscape of immune dysregulation in crohn's disease revealed through single-cell transcriptomic
571 profiling in the ileum and colon. *Immunity* **56**, 444–458 (2023).
- 572 44. Feldman, M., Friedman, L. S. & Brandt, L. J. *Sleisenger and Fordtran's gastrointestinal and liver disease E-book:*
573 *pathophysiology, diagnosis, management* (Elsevier health sciences, 2020).

- 574 45. Borenstein, M., Hedges, L. V., Higgins, J. P. & Rothstein, H. R. A basic introduction to fixed-effect and random-effects
575 models for meta-analysis. *Res. synthesis methods* **1**, 97–111 (2010).
- 576 46. Kenward, M. G. & Roger, J. H. Small sample inference for fixed effects from restricted maximum likelihood. *Biometrics*
577 **53**, 983–997 (1997).
- 578 47. Barrett, T. *et al.* Ncbi geo: archive for functional genomics data sets—update. *Nucleic Acids Res.* **41**, D991–D995 (2012).
- 579 48. Sayers, E. W. *et al.* Database resources of the national center for biotechnology information. *Nucleic Acids Res.* **47**,
580 D23–D28 (2019).
- 581 49. Kolesnikov, N. *et al.* Arrayexpress update—simplifying data submissions. *Nucleic Acids Res.* **43**, D1113–D1116 (2015).
- 582 50. Lewis, P. *et al.* Evidence for immune response, axonal dysfunction and reduced endocytosis in the substantia nigra in early
583 stage parkinson’s disease. *PLoS One* **10**, e0128651 (2015).
- 584 51. Cookson, M. R. *et al.* Systems-based analyses of brain regions functionally impacted in parkinson’s disease reveals
585 underlying causal mechanisms. *PLoS ONE* **9**, e102909 (2014).
- 586 52. Simchovitz, A. *et al.* A lncrna survey finds increases in neuroprotective linc-pint in parkinson’s disease substantia nigra.
587 *Aging Cell* **19**, e13115 (2020).
- 588 53. Duke, D. C., Moran, L. B., Pearce, R. K. B. & Graeber, M. B. The medial and lateral substantia nigra in parkinson’s
589 disease: mrna profiles associated with higher brain tissue vulnerability. *Neurogenetics* **8**, 83–94 (2007).
- 590 54. Leal, S. M. *et al.* A genomic pathway approach to a complex disease: axon guidance and parkinson disease. *PLoS Genet.*
591 **3**, e98 (2007).
- 592 55. Corradini, B. R. *et al.* Complex network-driven view of genomic mechanisms underlying parkinson’s disease: analyses in
593 dorsal motor vagal nucleus, locus coeruleus, and substantia nigra. *BioMed Res. Int.* **2014**, 1–16 (2014).
- 594 56. Zheng, B. *et al.* Pgc-1alpha, a potential therapeutic target for early intervention in parkinson’s disease. *Sci Transl Med* **2**,
595 52ra73 (2010).
- 596 57. Durrenberger, P. F. *et al.* Selection of novel reference genes for use in the human central nervous system: a brainnet europe
597 study. *Acta Neuropathol.* **124**, 893–903 (2012).
- 598 58. Cookson, M. R. *et al.* Srrm2, a potential blood biomarker revealing high alternative splicing in parkinson’s disease. *PLoS*
599 **One** **5**, e9104 (2010).
- 600 59. Scherzer, C. R. *et al.* Gata transcription factors directly regulate the parkinson’s disease-linked gene -synuclein. *Proc. Natl.*
601 *Acad. Sci.* **105**, 10907–10912 (2008).
- 602 60. Calligaris, R. *et al.* Blood transcriptomics of drug-naïve sporadic parkinson’s disease patients. *BMC Genomics* **16**, 876
603 (2015).
- 604 61. Mosley, R. L. *et al.* Biosignatures for parkinson’s disease and atypical parkinsonian disorders patients. *PLoS One* **7**,
605 e43595 (2012).
- 606 62. Locascio, J. J. *et al.* Association between -synuclein blood transcripts and early, neuroimaging-supported parkinson’s
607 disease. *Brain* **138**, 2659–2671 (2015).
- 608 63. Alieva, A. K. *et al.* Involvement of endocytosis and alternative splicing in the formation of the pathological process in the
609 early stages of parkinson’s disease. *BioMed Res. Int.* **2014**, 1–6 (2014).
- 610 64. Shamir, R. *et al.* Analysis of blood-based gene expression in idiopathic parkinson disease. *Neurology* **89**, 1676–1683
611 (2017).
- 612 65. Henderson, A. R. *et al.* Dna methylation and expression profiles of whole blood in parkinson’s disease. *Front. Genet.* **12**,
613 640266 (2021).
- 614 66. Planell, N. *et al.* Usefulness of transcriptional blood biomarkers as a non-invasive surrogate marker of mucosal healing and
615 endoscopic response in ulcerative colitis. *J. Crohn’s Colitis* **11**, 1335–1346 (2017).
- 616 67. Mo, A. *et al.* Disease-specific regulation of gene expression in a comparative analysis of juvenile idiopathic arthritis and
617 inflammatory bowel disease. *Genome Medicine* **10**, 48 (2018).
- 618 68. Ostrowski, J. *et al.* Common functional alterations identified in blood transcriptome of autoimmune cholestatic liver and
619 inflammatory bowel diseases. *Sci. Reports* **9**, 7190 (2019).
- 620 69. Haberman, Y. *et al.* Pediatric crohn disease patients exhibit specific ileal transcriptome and microbiome signature. *J. Clin.*
621 *Investig.* **124**, 3617–3633 (2014).

- 622 70. Haberman, Y. *et al.* Age-of-diagnosis dependent ileal immune intensification and reduced alpha-defensin in older versus
623 younger pediatric crohn disease patients despite already established dysbiosis. *Mucosal Immunol.* **12**, 491–502 (2019).
- 624 71. Pérez-Torras, S. *et al.* Transportome profiling identifies profound alterations in crohn's disease partially restored by
625 commensal bacteria. *J. Crohn's Colitis* **10**, 850–859 (2016).
- 626 72. Verstockt, S. *et al.* Gene and mirna regulatory networks during different stages of crohn's disease. *J. Crohn's Colitis* **13**,
627 916–930 (2019).
- 628 73. Timmer, A. *et al.* Mucosal gene expression of antimicrobial peptides in inflammatory bowel disease before and after first
629 infliximab treatment. *PLoS One* **4**, e7984 (2009).
- 630 74. Vancamelbeke, M. *et al.* Genetic and transcriptomic bases of intestinal epithelial barrier dysfunction in inflammatory
631 bowel disease. *Inflamm. Bowel Dis.* **23**, 1718–1729 (2017).
- 632 75. van Beelen Granlund, A. *et al.* Reg gene expression in inflamed and healthy colon mucosa explored by in situ hybridisation.
633 *Cell Tissue Res.* **352**, 639–646 (2013).
- 634 76. Carey, R. *et al.* Activation of an il-6:stat3-dependent transcriptome in pediatric-onset inflammatory bowel disease. *Inflamm.*
635 *Bowel Dis.* **14**, 446–457 (2008).
- 636 77. Galamb, O. *et al.* Inflammation, adenoma and cancer: objective classification of colon biopsy specimens with gene
637 expression signature. *Dis. Markers* **25**, 1–16 (2008).
- 638 78. Calogero, R. A. *et al.* Identification of novel predictor classifiers for inflammatory bowel disease by gene expression
639 profiling. *PLoS One* **8**, e76235 (2013).
- 640 79. Peck, B. C. E. *et al.* Micrornas classify different disease behavior phenotypes of crohns disease and may have prognostic
641 utility. *Inflamm. Bowel Dis.* **21**, 2178–2187 (2015).
- 642 80. Gentleman, R., Carey, V., Huber, W., Irizarry, R. & Dudoit, S. *Bioinformatics and computational biology solutions using R*
643 *and Bioconductor* (Springer Science & Business Media, 2005).
- 644 81. Ritchie, M. E. *et al.* limma powers differential expression analyses for rna-sequencing and microarray studies. *Nucleic*
645 *Acids Res.* **43**, e47–e47 (2015).
- 646 82. Köster, J. & Rahmann, S. Snakemake—a scalable bioinformatics workflow engine. *Bioinformatics* **28**, 2520–2522 (2012).
- 647 83. Bolger, A. M., Lohse, M. & Usadel, B. Trimmomatic: a flexible trimmer for illumina sequence data. *Bioinformatics* **30**,
648 2114–2120 (2014).
- 649 84. Sahraeian, S. M. E. *et al.* Gaining comprehensive biological insight into the transcriptome by performing a broad-spectrum
650 rna-seq analysis. *Nat. Commun.* **8**, 59 (2017).
- 651 85. Kim, D., Paggi, J. M., Park, C., Bennett, C. & Salzberg, S. L. Graph-based genome alignment and genotyping with hisat2
652 and hisat-genotype. *Nat. Biotechnol.* **37**, 907–915 (2019).
- 653 86. Liao, Y., Smyth, G. K. & Shi, W. featurecounts: an efficient general purpose program for assigning sequence reads to
654 genomic features. *Bioinformatics* **30**, 923–930 (2014).
- 655 87. Love, M. I., Huber, W. & Anders, S. Moderated estimation of fold change and dispersion for rna-seq data with deseq2.
656 *Genome biology* **15**, 1–21 (2014).
- 657 88. Yang, X., Bentink, S., Scheid, S. & Spang, R. Similarities of ordered gene lists. *J. Bioinforma. Comput. Biol.* **4**, 693–708
658 (2011).
- 659 89. Piñero, J. *et al.* The disgenet knowledge platform for disease genomics: 2019 update. *Nucleic acids research* **48**,
660 D845–D855 (2020).
- 661 90. Yuan, X. *et al.* The common genes involved in the pathogenesis of alzheimer's disease and type 2 diabetes and their
662 implication for drug repositioning. *Neuropharmacology* **223**, 109327 (2023).
- 663 91. Ferreira, J. C., Alshamali, F., Pereira, L. & Fernandes, V. Characterization of arabian peninsula whole exomes: contributing
664 to the catalogue of human diversity. *iScience* **25**, 105336 (2022).
- 665 92. Rappaport, N. *et al.* Malacards: an amalgamated human disease compendium with diverse clinical and genetic annotation
666 and structured search. *Nucleic acids research* **45**, D877–D887 (2017).

667 **Acknowledgements**

668 The authors thank all members from Ming Chen's Group of Bioinformatics for insightful discussions. This work was supported
669 by the National Key Research and Development Program of China (2023YFE0112300); National Natural Sciences Foundation
670 of China (32261133526; 32270709; 32070677); the 151 talent project of Zhejiang Province (first level), the Science and
671 Technology Innovation Leading Scientist (2022R52035).

672 **Author contributions**

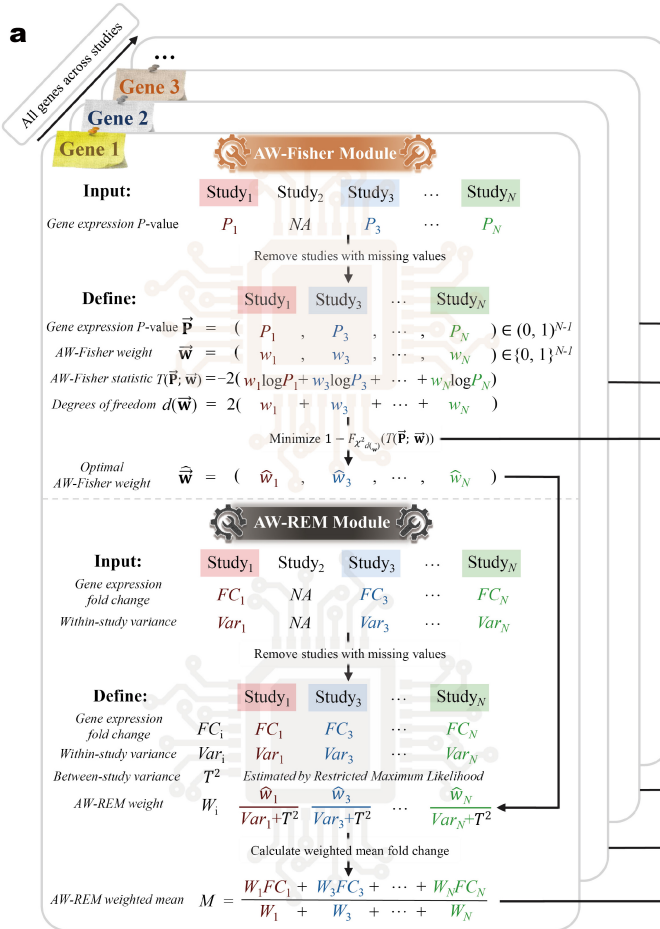
673 Y.S.H. conceptualized the study. M.C. supervised the study. Y.S.H., Z.W., and Y.H. performed data analysis. Y.S.H., Z.W., C.F.,
674 and Q.F. contributed to writing the manuscript. All authors reviewed and approved the final manuscript.

675 **Competing interests**

676 The authors declare no competing interests.

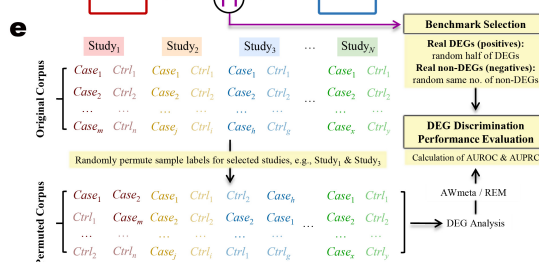
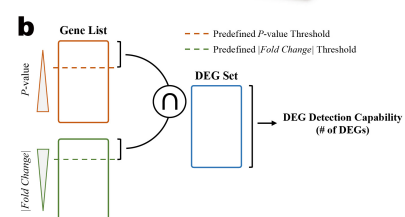
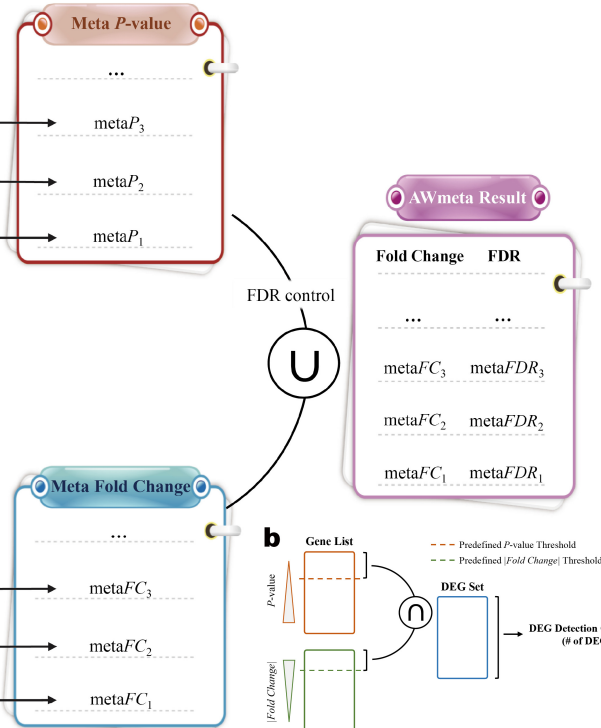
677 **Publisher's note**

678 Springer Nature remains neutral with regard to jurisdictional claims in published maps and institutional affiliations.



AWmeta

Empowering adaptively-weighted meta-analysis
for transcriptomic data



f Study Permutation Statistics in DEG Discrimination Evaluation

Disease Tissue	Min. No.	Median No.	Max. No.
Parkinson's substantia nigra	1	3	5
Parkinson's peripheral blood	1	2	3
Crohn's peripheral blood	1	1	1
Crohn's ileal mucosa	1	2	2
Crohn's colonic mucosa	1	3	3

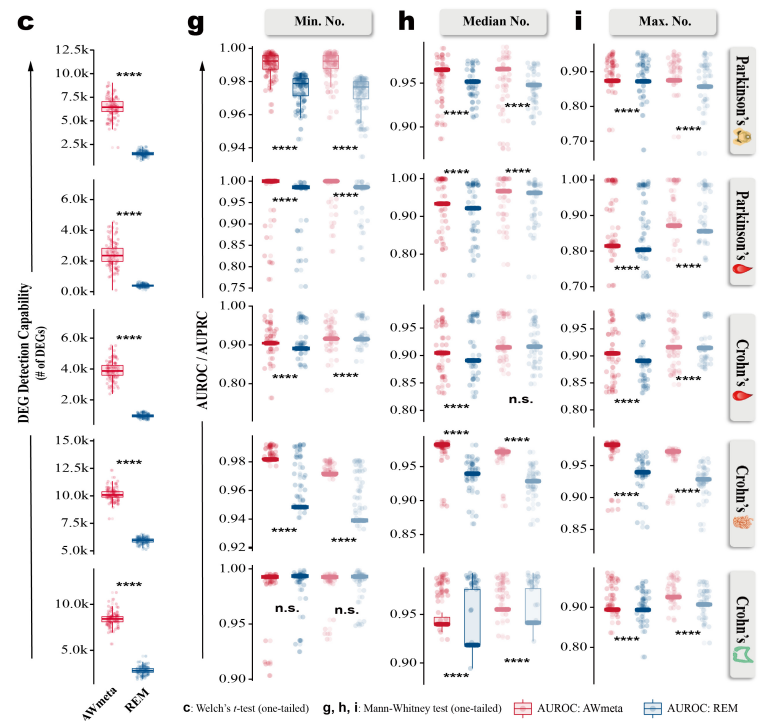


Fig. 1 | Overview of AWmeta and DEG identification evaluation. **a**, Schematic of the AWmeta framework, comprising the AW-Fisher module for *P*-value calculation and the AW-REM module for effect size (\log_2 -transformed fold change) estimation. DEG identification evaluation includes DEG detection capability (**b**, **c**) and discrimination (**d–i**). **b**, Schematic defining DEG detection capability as the number of DEGs identified by predefined statistical significance (*P*-value) and gene expression fold change (\log_2 -based) thresholds. **c**, DEG detection capability performance comparisons between AWmeta and REM with corrected *P*-value (FDR) < 0.01 and fold change ($|log_2FC|$) > $\log_2 1.2$ across five disease tissues. Statistical significance was determined with one-tailed Welch's *t*-test. **d**, Strategy for generating the semi-synthetic benchmark dataset, sampling equivalent DEGs and non-DEGs from common genes identified by both AWmeta and REM. **e**, Workflow for evaluating DEG discrimination performance using sample label permutation within the semi-synthetic benchmark dataset, followed by AWmeta/REM procedure and AUROC/AUPRC calculation. **f**, Study permutation statistics (number of permuted studies) in the DEG discrimination evaluation procedure across five disease tissues. **g–i**, DEG discrimination performance comparisons between AWmeta and REM using minimum- (**g**), median- (**h**), and maximum- (**i**) permuted semi-synthetic simulation strategy with FDR < 0.01 and $|log_2FC|$ > $\log_2 1.2$ across five disease tissues. Statistical significance was determined using one-tailed Mann-Whitney test (**g–i**). Textual details of the AWmeta framework, DEG detection capability, and minimum-, median- and maximum-permuted semi-synthetic simulation strategies for DEG discrimination, reside in "DEG detection capability evaluation" and "DEG discrimination evaluation using semi-synthetic simulation strategy" sections in Methods. Boxplot bounds indicate interquartile ranges (IQR), centers denote median values, and whiskers extend to $1.5 \times$ IQR. The following icons represent different tissue sources: 🧠: substantia nigra; 💊: peripheral blood; 🍆: ileal mucosa; 🌿: colonic mucosa.

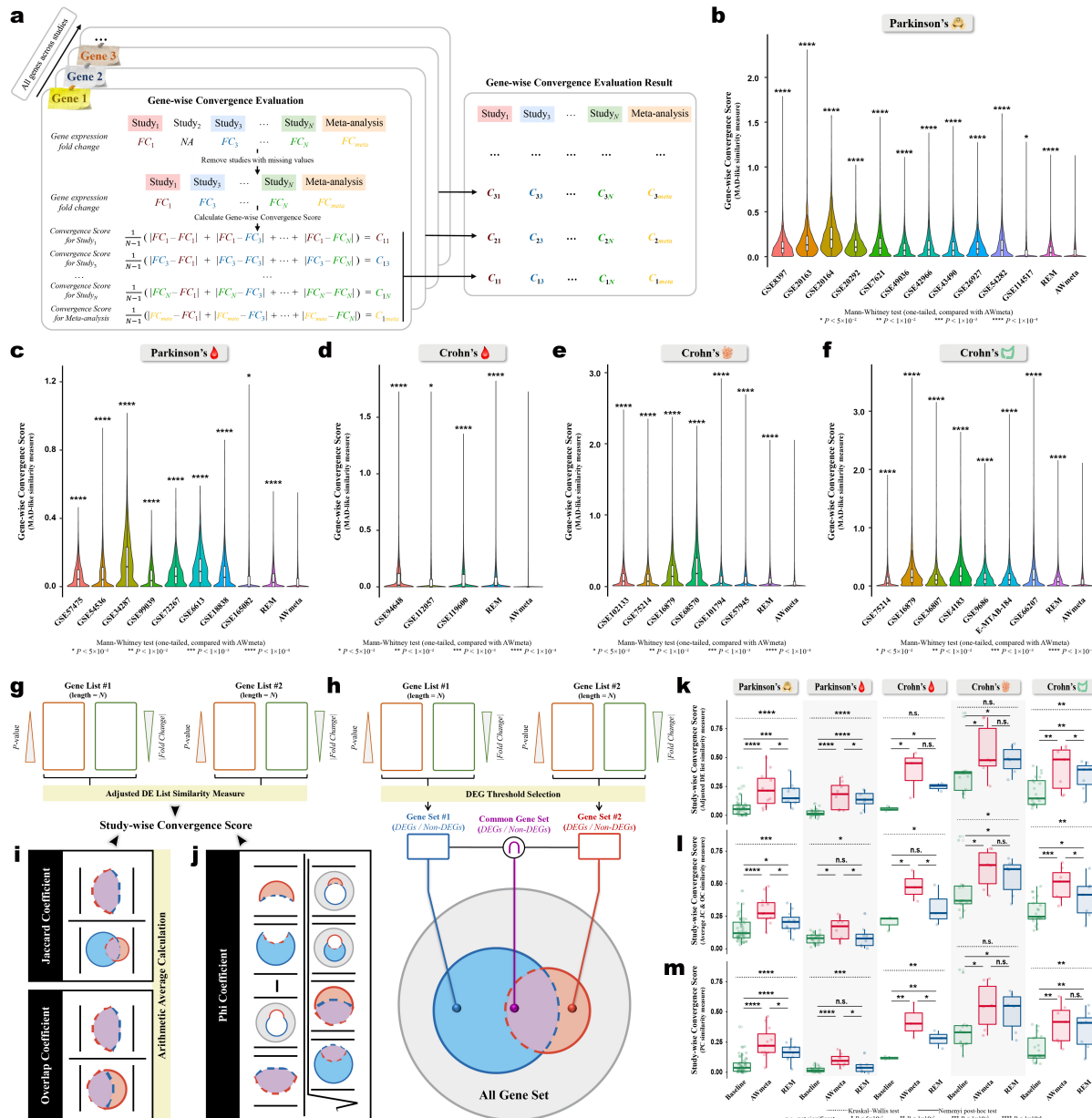


Fig. 2 | AWmeta establishes superior gene- and study-wise convergence in gene differential quantification. To benchmark meta-analysis efficacy across biological scales, we assessed gene differential quantification convergence in gene- (**a–f**) and study- (**g–m**) wise manners. **a–f**, For gene-wise convergence, mean absolute deviation (MAD)-like similarity measure was utilized to quantify the per-gene fold change (\log_2FC) similarity among AWmeta, REM and original studies (**a**), with smaller value indicating better convergence, which demonstrates AWmeta's superior gene-wise convergence over REM and original studies across five disease tissues: Parkinson's substantia nigra (**b**) and peripheral blood (**c**), and Crohn's peripheral blood (**d**), ileal mucosa (**e**) and colonic mucosa (**f**). Statistical significance against AWmeta for gene-wise convergence comparisons was determined by one-tailed Mann-Whitney test. **g–m**, Three complementary similarities, i.e., adjusted DE list similarity (**g**, conceptual schematic; **k**, assessment result), the arithmetic average of Jaccard (JC) and overlap coefficient (OC) (**h**, **i**, conceptual schematic; **l**, assessment result) and phi coefficient (PC) (**h**, **j**, conceptual schematic; **m**, assessment result), were used to derive study-wise convergence score, indicating AWmeta exerts better convergence than REM and baselines in five disease tissues with FDR < 0.05 and $\log_2FC > \log_21.2$. For comparison purpose, results from original studies serve as reference baselines. Overall study-wise convergence differences among AWmeta, REM and baselines were tested with Kruskal-Wallis test, followed by Nemenyi post-hoc test for pairwise comparisons. Detailed description for MAD-like gene- and three study-wise convergence similarity measures can be referred to in "Gene-wise convergence assessment for gene differential quantification" and "Study-wise convergence assessment for gene differential quantification" sections in Methods and Extended Data Fig. 7. Boxplot bounds show interquartile ranges (IQR), centers indicate median values, and whiskers extend to $1.5 \times IQR$. The following icons represent different tissue sources: 🧠: substantia nigra; 💯: peripheral blood; 🍆: ileal mucosa; 🌿: colonic mucosa.

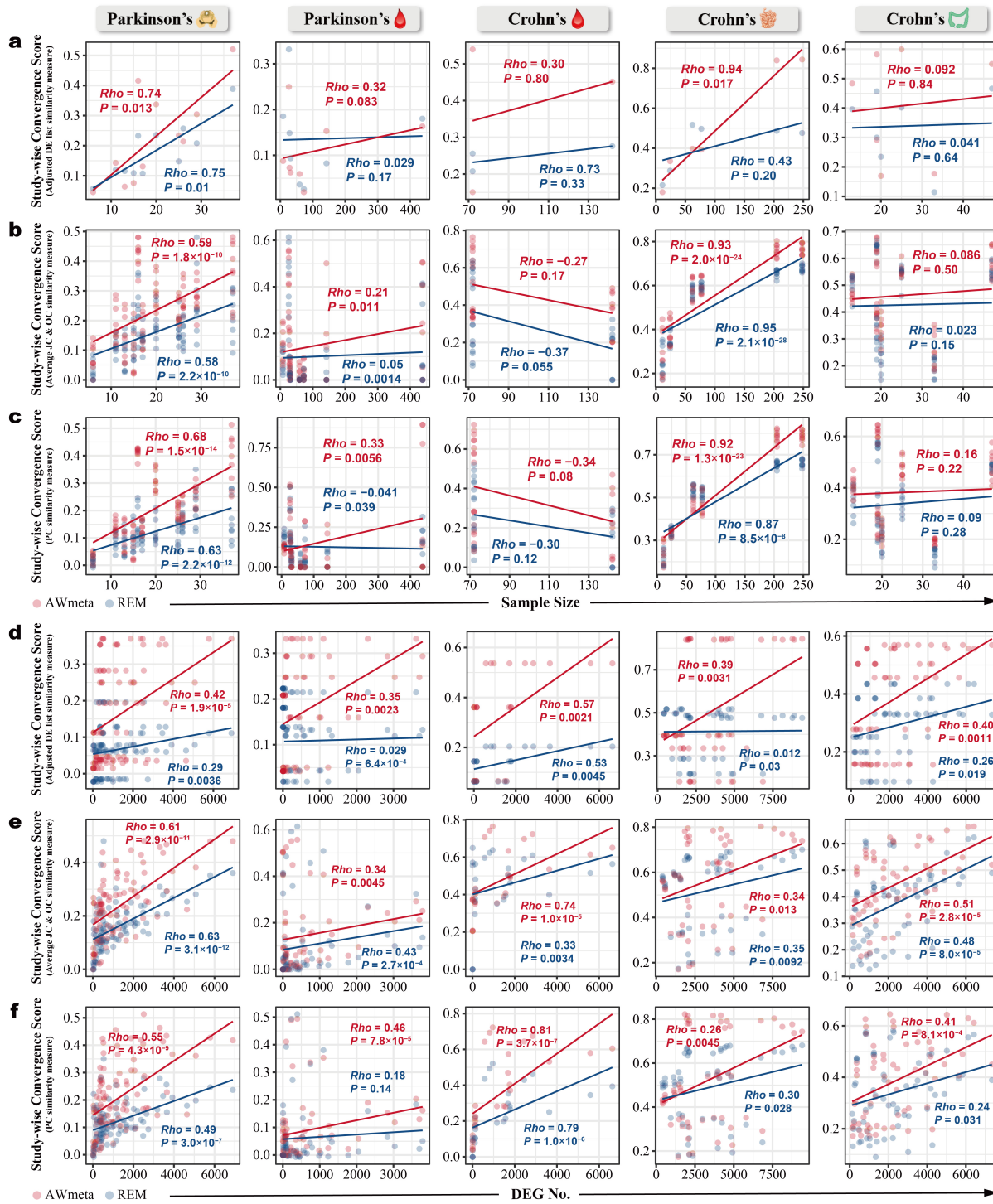


Fig. 3 | AWmeta attains accelerated meta-analysis convergence with reduced samples and DEGs. a–f, We dissected the correlations of per-study sample size and DEG number with study-wise convergence measured by three complementary similarities, i.e., adjusted DE list similarity (**a**, **d**), the arithmetic average of Jaccard (JC) and overlap coefficient (OC) (**b**, **e**) and phi coefficient (PC) (**c**, **f**) across five disease tissues, showcasing AWmeta’s accelerated study-wise meta-analysis convergence against REM with fewer samples and DEGs, in which non-linear correlations were quantified by spearman’s rho with two-tailed significance test. To enhance statistical power and mitigate threshold sensitivity, this correlation analysis summarized results from nine different DEG threshold combinations, spanning varying significance levels (0.01, 0.05 and 0.10) and fold change cutoffs ($\log_2 1.2$, $\log_2 1.5$ and $\log_2 2.0$), for both the average of JC and OC and PC similarity measures. Detailed description for these three study-wise convergence similarity measures can be referred to in "Study-wise convergence assessment for gene differential quantification" section in Methods, Fig. 2g–j and Extended Data Fig. 7. The following icons represent different tissue sources: 🍂: substantia nigra; 💯: peripheral blood; 🍄: ileal mucosa; 🌿: colonic mucosa.

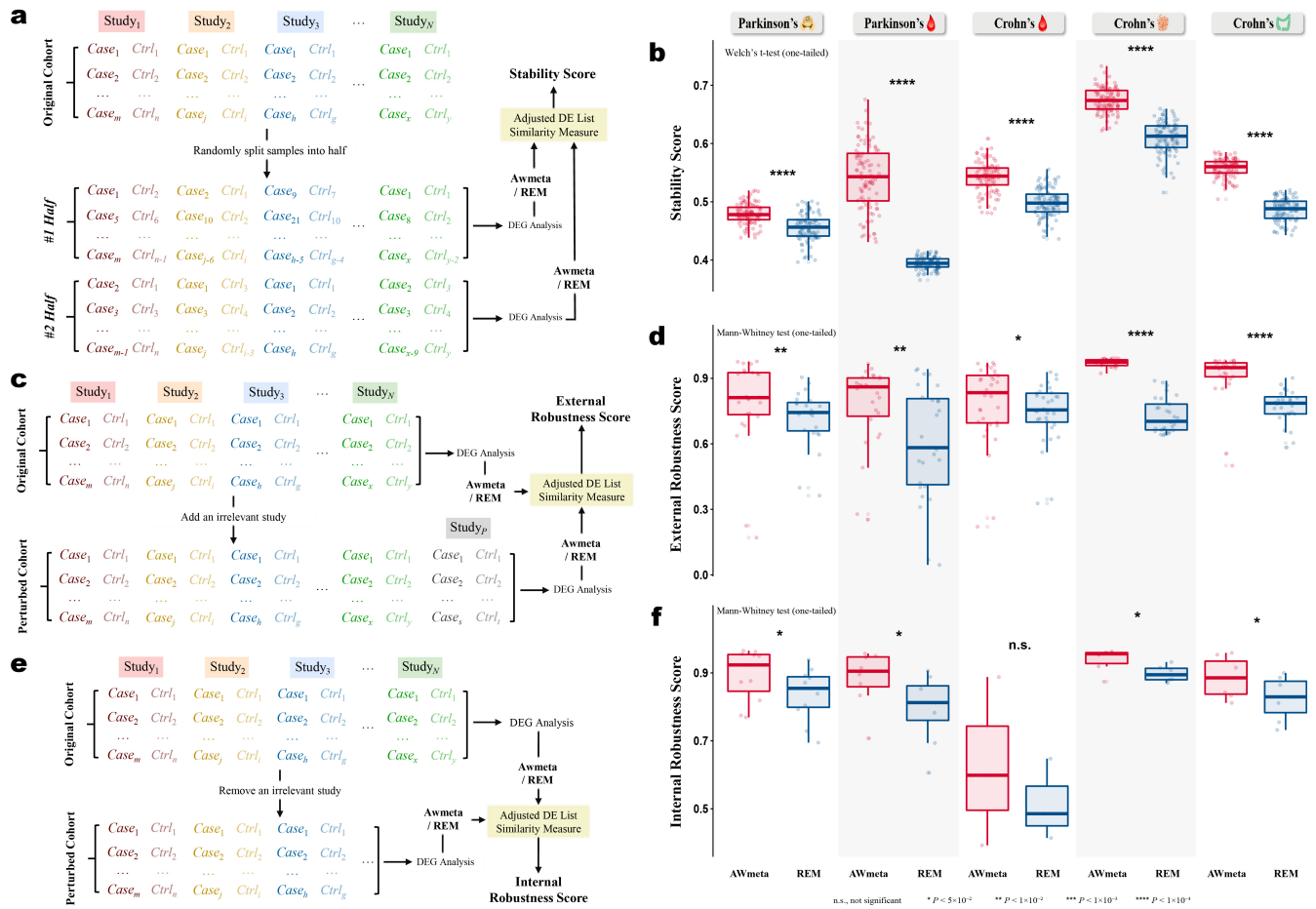


Fig. 4 | AWmeta delivers remarkable stability and robustness in transcriptomic integration. **a**, Workflow for evaluating the stability of transcriptomic integration. **b**, Stability assessment against AWmeta and REM with one-tailed Welch's *t*-test. **c–f**, We assessed robustness against external interference (**c**, conceptual schematic; **d**, assessment result) and internal defects (**e**, conceptual schematic; **f**, assessment result) in transcriptomic integration across five disease tissues, with one-tailed Mann-Whitney test, indicating AWmeta's superior performance over REM. Detailed description of adjusted DE list similarity measure can be referred to in "Study-wise convergence assessment for gene differential quantification" section in Methods and Extended Data Fig. 7. Boxplot bounds show interquartile ranges (IQR), centers indicate median values, and whiskers extend to $1.5 \times \text{IQR}$. The following icons represent different tissue sources: 🧠: substantia nigra; 💓: peripheral blood; 🍆: ileal mucosa; 🌐: colonic mucosa.

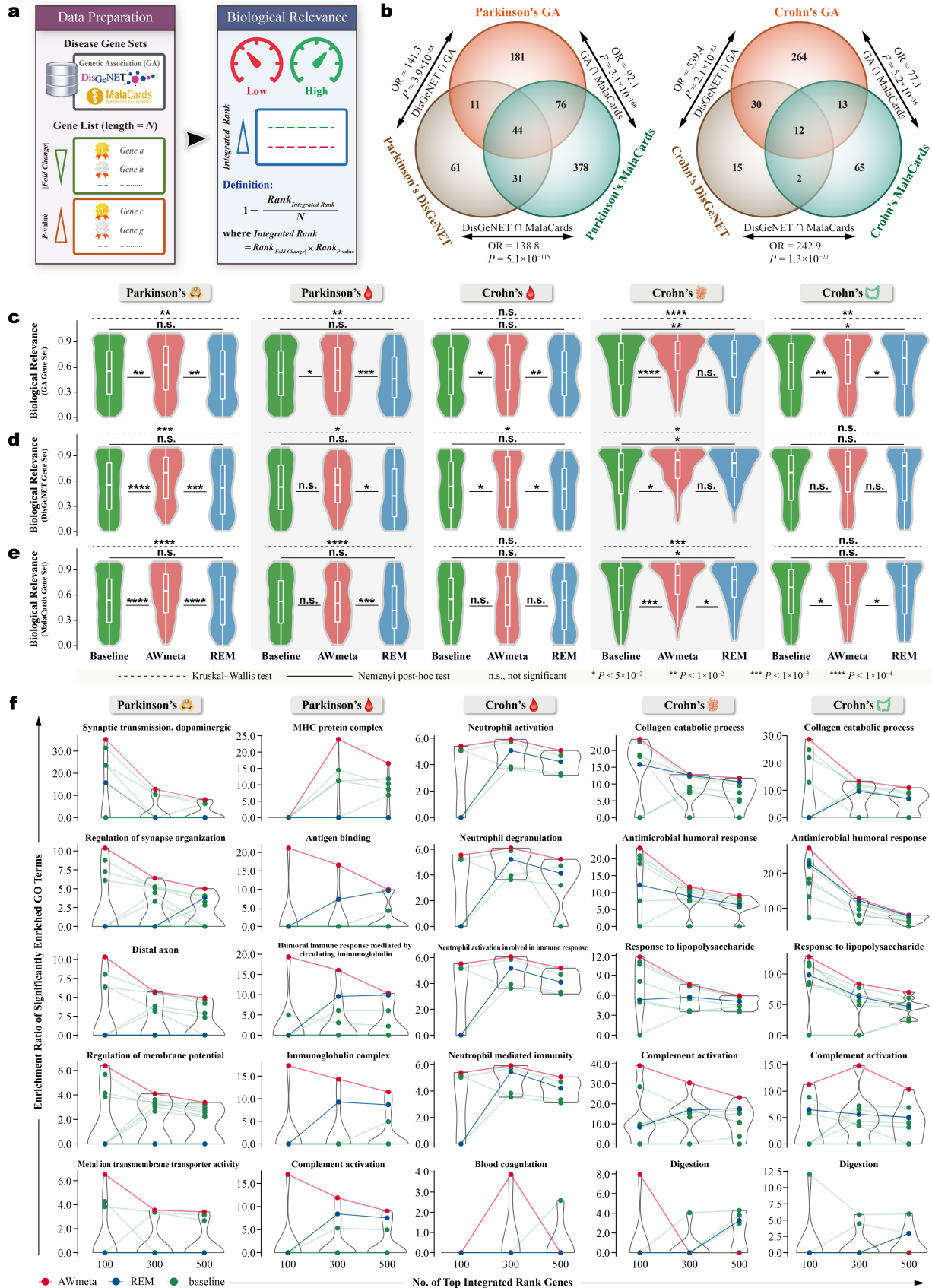
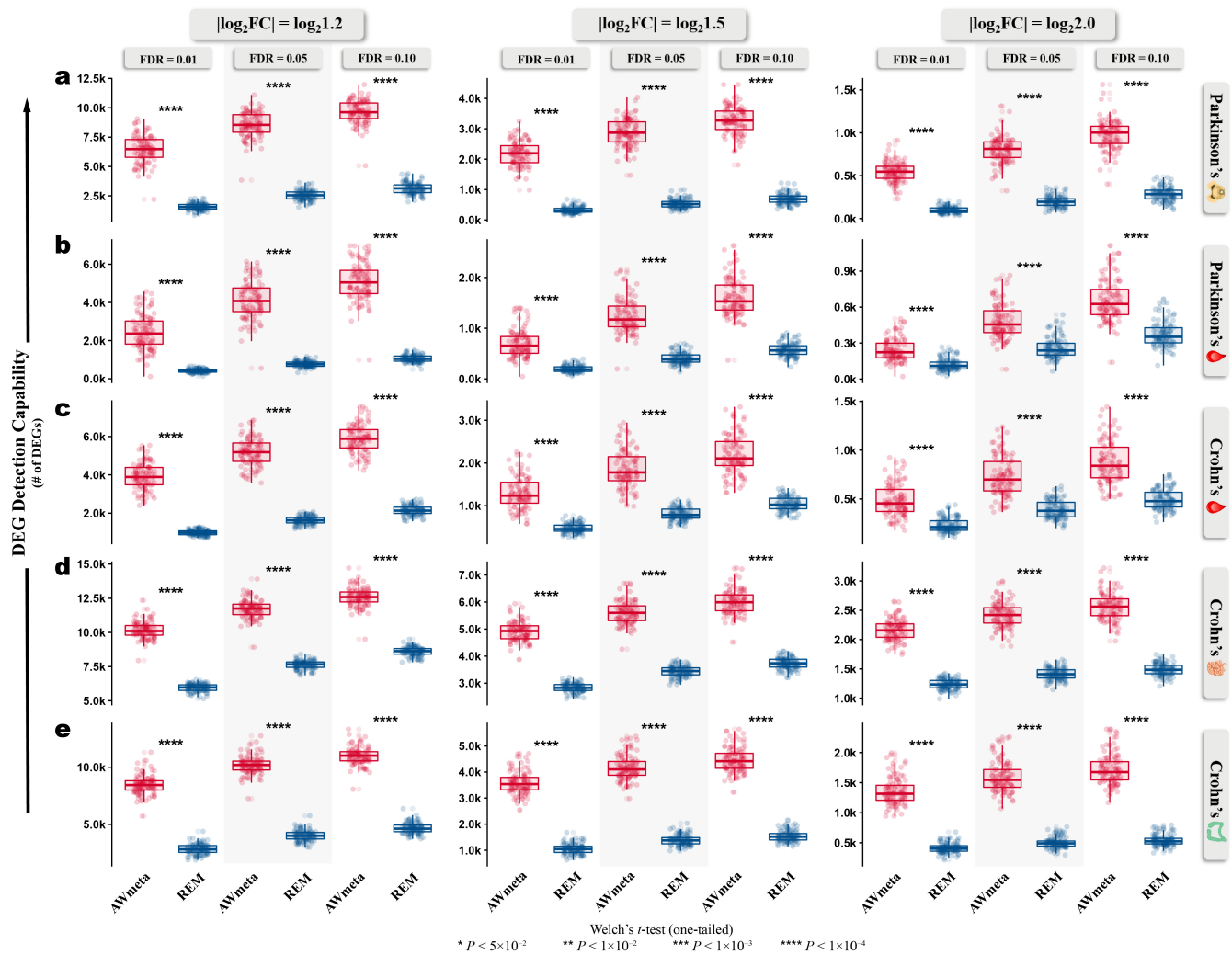


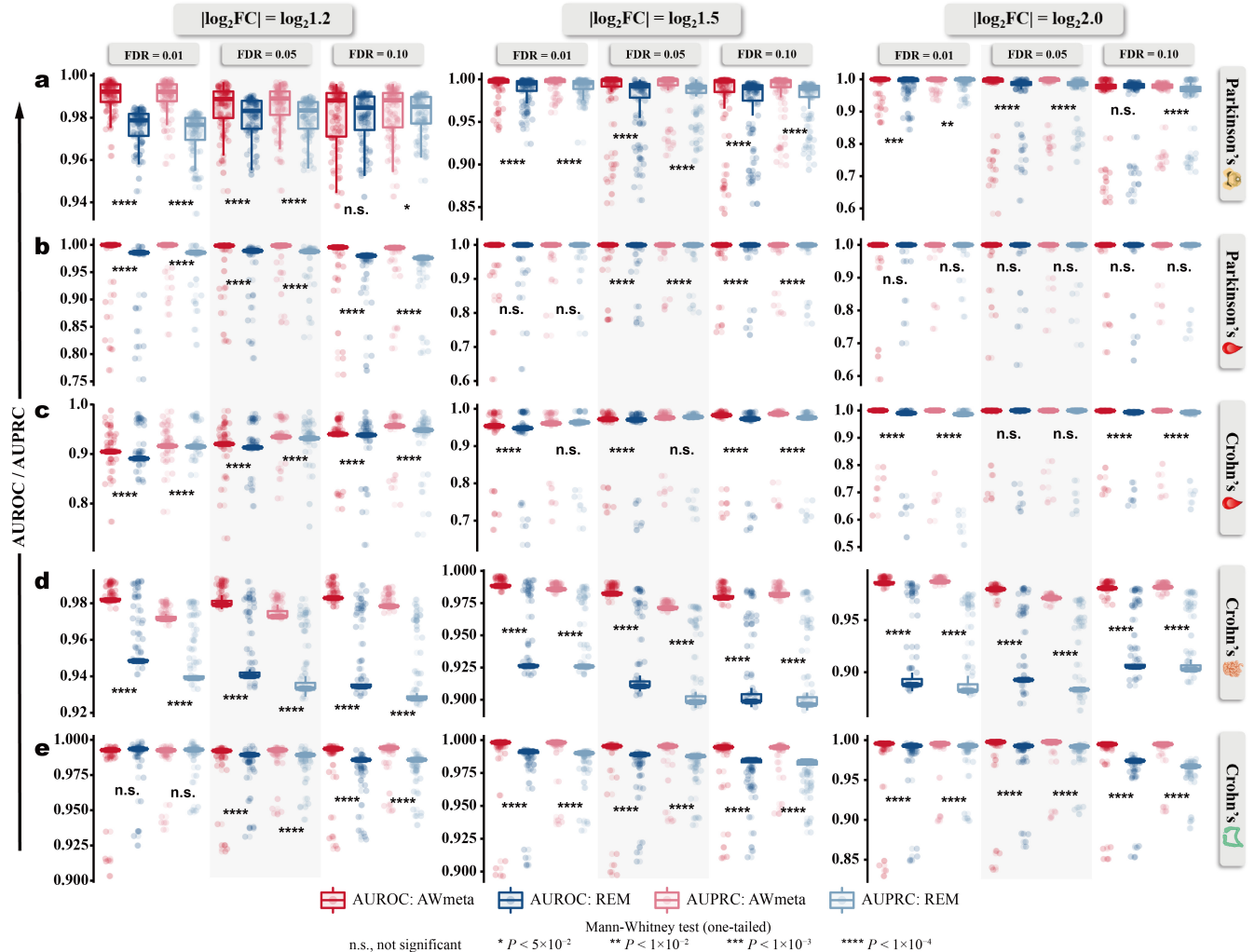
Fig. 5 | AWmeta enhances identification and mechanism interpretation of disease tissue-specific genes. **a**, Workflow for quantifying gene-wise biological relevance against three benchmark gene sets of Parkinson's and Crohn's disease from genetic association (GA) variation corpus, DisGeNET and MalaCards, with higher scores indicating stronger tissue-contextual disease associations. **b**, Pairwise coherence analysis of the three benchmark gene sets for Parkinson's and Crohn's disease. The degree of overlap between benchmarks was quantified using odds ratios (OR), with statistical significance determined by Fisher's exact test. **c–e**, Biological relevance evaluations on AWmeta (red), REM (blue) and baselines (green) against GA (**c**), DisGeNET (**d**) and MalaCards (**e**) benchmarks, where higher scores (y-axis) denote enhanced biological relevance. Original study-derived biological relevance results serve as reference baselines. We assessed overall differences in biological relevance scores using Kruskal-Wallis test, with Nemenyi post-hoc test for pairwise comparisons (AWmeta versus REM, AWmeta versus baseline, and REM versus baseline). Boxplot bounds indicate interquartile ranges (IQR), centers denote median values, and whiskers extend to $1.5 \times \text{IQR}$. **f**, Dynamic GO enrichment trajectories across top-ranked (100, 300 and 500) genes identified by AWmeta (red), REM (blue) and baselines (green), with higher enrichment ratio (y-axis) indicating stronger disease-tissue involvement. Original study-derived enrichments serve as baselines. Connected lines visualize trajectory patterns across gene rank thresholds (x-axis). Textual details of the biological relevance assessment framework and detailed definition of enrichment ratio, reside in "Biological relevance assessment of gene differential quantification" section in Methods and "AWmeta enables disease tissue-specific mechanism interpretation" section in Results. The following icons represent different tissue sources: 🧠: substantia nigra; 💉: Peripheral blood; 🍆: ileal mucosa; 🌱: colonic mucosa.

Dataset	Sequencing platform	Dataset source	Tissue source	Samples
Data IDs	Microarray or next-generation sequencing platforms	GEO, SRA and ArrayExpress	Blood, SN, IM and CM	No. of patients versus normals
PD datasets				
GSE57475	Illumina HumanHT-12 V3.0 expression beadchip	Gene Expression Omnibus		93 versus 49
GSE54536	Illumina HumanHT-12 V4.0 expression beadchip	Gene Expression Omnibus		4 versus 4
GSE34287	ExonHit Human Genome Wide SpliceArray 1.0	Gene Expression Omnibus		19 versus 12
GSE99039	Affymetrix Human Genome U133 Plus 2.0 Array	Gene Expression Omnibus		205 versus 233
GSE72267	Affymetrix Human Genome U133A 2.0 Array	Gene Expression Omnibus		40 versus 19
GSE6613	Affymetrix Human Genome U133A Array	Gene Expression Omnibus		50 versus 22
GSE18838	Affymetrix Human Exon 1.0 ST Array	Gene Expression Omnibus		17 versus 11
GSE165082	Illumina HiSeq 2000	Gene Expression Omnibus		12 versus 14
GSE114517	Illumina NextSeq 500	Gene Expression Omnibus		17 versus 12
GSE8397	Affymetrix Human Genome U133A Array	Gene Expression Omnibus		24 versus 13
GSE20163	Affymetrix Human Genome U133A Array	Gene Expression Omnibus		8 versus 9
GSE20164	Affymetrix Human Genome U133A Array	Gene Expression Omnibus		6 versus 5
GSE20292	Affymetrix Human Genome U133A Array	Gene Expression Omnibus		11 versus 15
GSE7621	Affymetrix Human Genome U133 Plus 2.0 Array	Gene Expression Omnibus		16 versus 9
GSE49036	Affymetrix Human Genome U133 Plus 2.0 Array	Gene Expression Omnibus		8 versus 8
GSE42966	Agilent-014850 Whole Human Genome Microarray 4x44K G4112F	Gene Expression Omnibus		9 versus 6
GSE43490	Agilent-014850 Whole Human Genome Microarray 4x44K G4112F	Gene Expression Omnibus		8 versus 5
GSE26927	Illumina humanRef-8 v2.0 expression beadchip	Gene Expression Omnibus		12 versus 8
GSE54282	Affymetrix Human Gene 1.0 ST Array	Gene Expression Omnibus		3 versus 3
CD datasets				
GSE119600	Illumina HumanHT-12 V4.0 expression beadchip	Gene Expression Omnibus		95 versus 47
GSE112057	Illumina HiSeq 2000	Gene Expression Omnibus		60 versus 12
GSE94648	Affymetrix Human Genome U133 Plus 2.0 Array	Gene Expression Omnibus		50 versus 22
GSE102133	Affymetrix Human Gene 1.0 ST Array	Gene Expression Omnibus		65 versus 12
GSE75214	Affymetrix Human Gene 1.0 ST Array	Gene Expression Omnibus		51 versus 11
GSE16879	Affymetrix Human Genome U133 Plus 2.0 Array	Gene Expression Omnibus		18 versus 6
GSE68570	Illumina HumanHT-12 V4.0 expression beadchip	Gene Expression Omnibus		6 versus 5
GSE101794	Illumina HiSeq 2000	Gene Expression Omnibus		198 versus 50
GSE57945	Illumina HiSeq 2000	Gene Expression Omnibus		163 versus 42
GSE75214	Affymetrix Human Gene 1.0 ST Array	Gene Expression Omnibus		8 versus 11
GSE16879	Affymetrix Human Genome U133 Plus 2.0 Array	Gene Expression Omnibus		19 versus 6
GSE36807	Affymetrix Human Genome U133 Plus 2.0 Array	Gene Expression Omnibus		13 versus 7
GSE4183	Affymetrix Human Genome U133 Plus 2.0 Array	Gene Expression Omnibus		5 versus 8
GSE9686	Affymetrix Human Genome U133 Plus 2.0 Array	Gene Expression Omnibus		11 versus 8
E-MTAB-184	Illumina HumanHT-12 v3.0 expression beadChip	Gene Expression Omnibus		15 versus 32
GSE66207	Illumina HiSeq 2500	Gene Expression Omnibus		20 versus 13
No. of Parkinson's (PD) / Crohn's disease (CD) patients:				
4 8 16 32 64 128 256				
No. of normals:				
4 8 16 32 64 128				
GEO SRA ArrayExpress Peripheral blood Substantia nigra (SN) Ileal mucosa (IM) Colonic mucosa (CM)				
No. of PD / CD patients				
No. of normals				

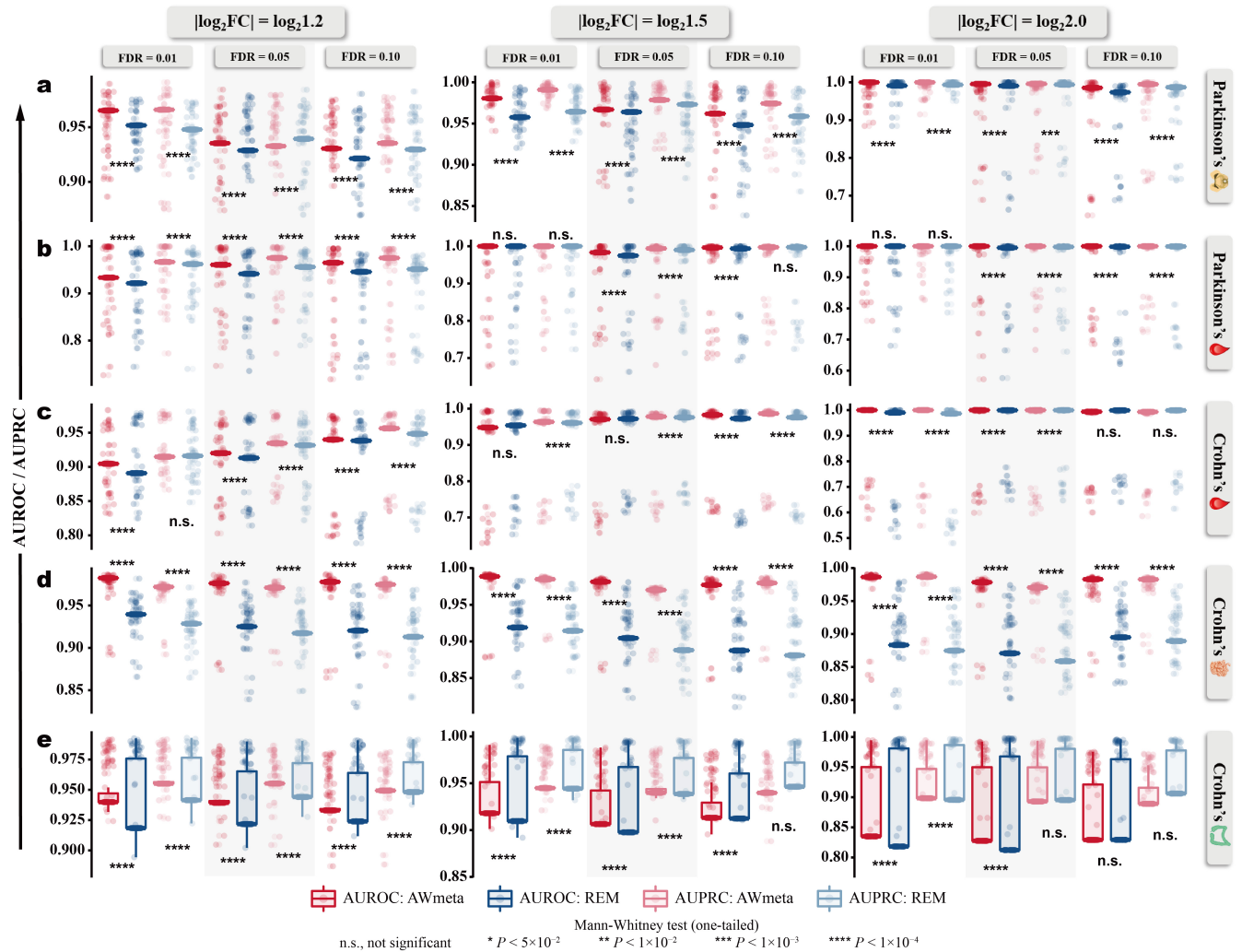
Extended Data Fig. 1 | Overview of transcriptomic datasets for Parkinson's and Crohn's disease. Datasets for Parkinson's disease (PD) include substantia nigra^{50–57} and peripheral blood^{53,58–65}. Crohn's disease (CD) datasets comprise ileal mucosa^{69–74}, colonic mucosa^{73–79}, and peripheral blood^{66–68}. Detailed metadata include data accession IDs, sequencing platform identifiers, dataset and tissue sources, and patient and control sample sizes. The following icons represent different tissue sources: : substantia nigra (SN); : peripheral blood; : ileal mucosa (IM); : colonic mucosa (CM).

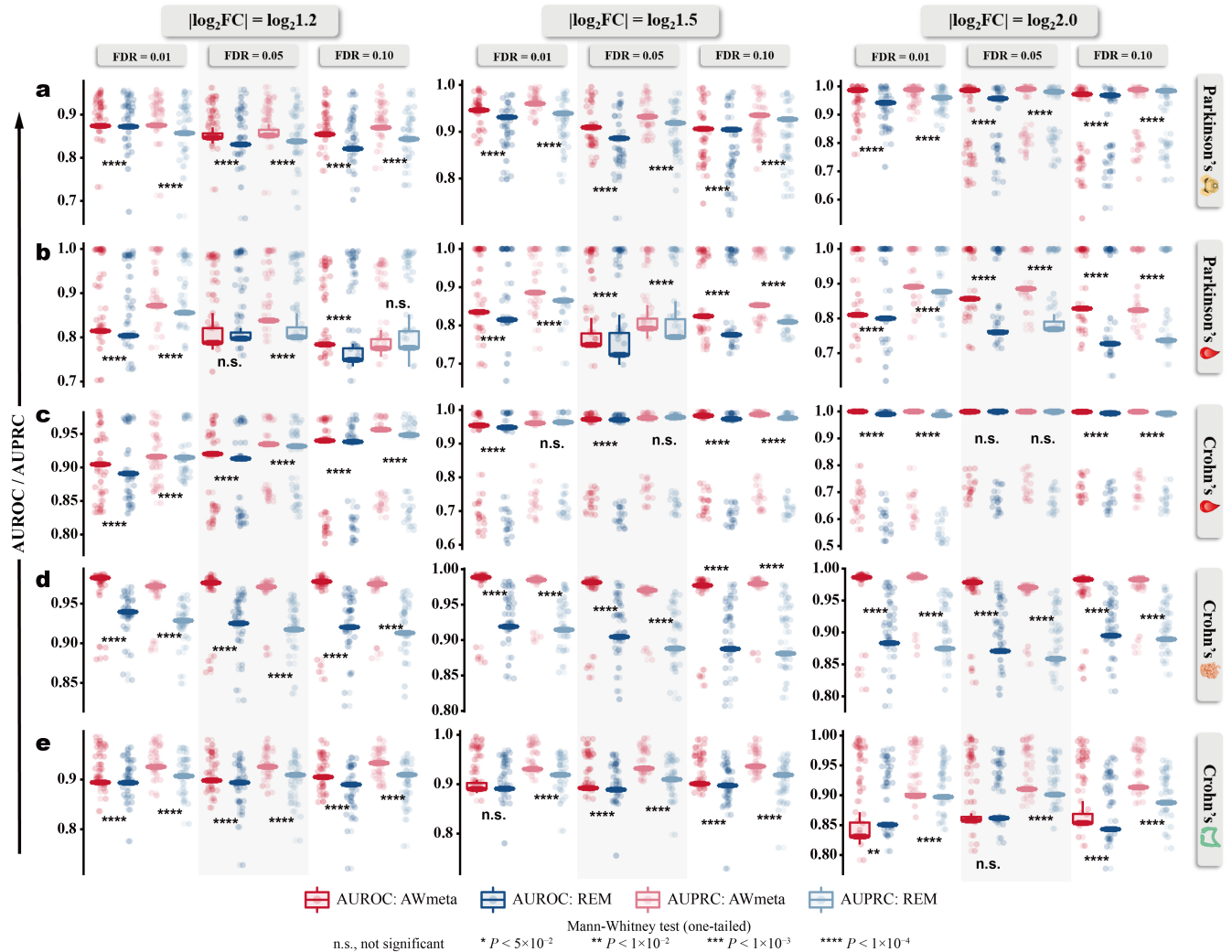


Extended Data Fig. 2 | DEG detection capability evaluation across five disease tissues and diverse thresholds. **a–e**, DEG detection capability (the number of identified DEGs) was assessed against AWMeta and REM using nine distinct thresholds, combining three corrected *P*-values (FDR) (0.01, 0.05, and 0.10) and three log₂-based fold change (log₂FC) cutoffs (log₂1.2, log₂1.5, and log₂2.0), spanning Parkinson's substantia nigra (**a**), Parkinson's (**b**) and Crohn's (**c**) peripheral blood, and Crohn's ileal (**d**) and colonic (**e**) mucosa. Detailed description of DEG detection capability can be referred to in "DEG detection capability evaluation" section in Methods and Fig. 1b. Statistical significance was determined using one-tailed Welch's *t*-test. Boxplot bounds show interquartile ranges (IQR), centers indicate median values, and whiskers extend to 1.5×IQR. The following icons represent different tissue sources: 🧠: substantia nigra; 💊: peripheral blood; 🍆: ileal mucosa; 🌿: colonic mucosa.

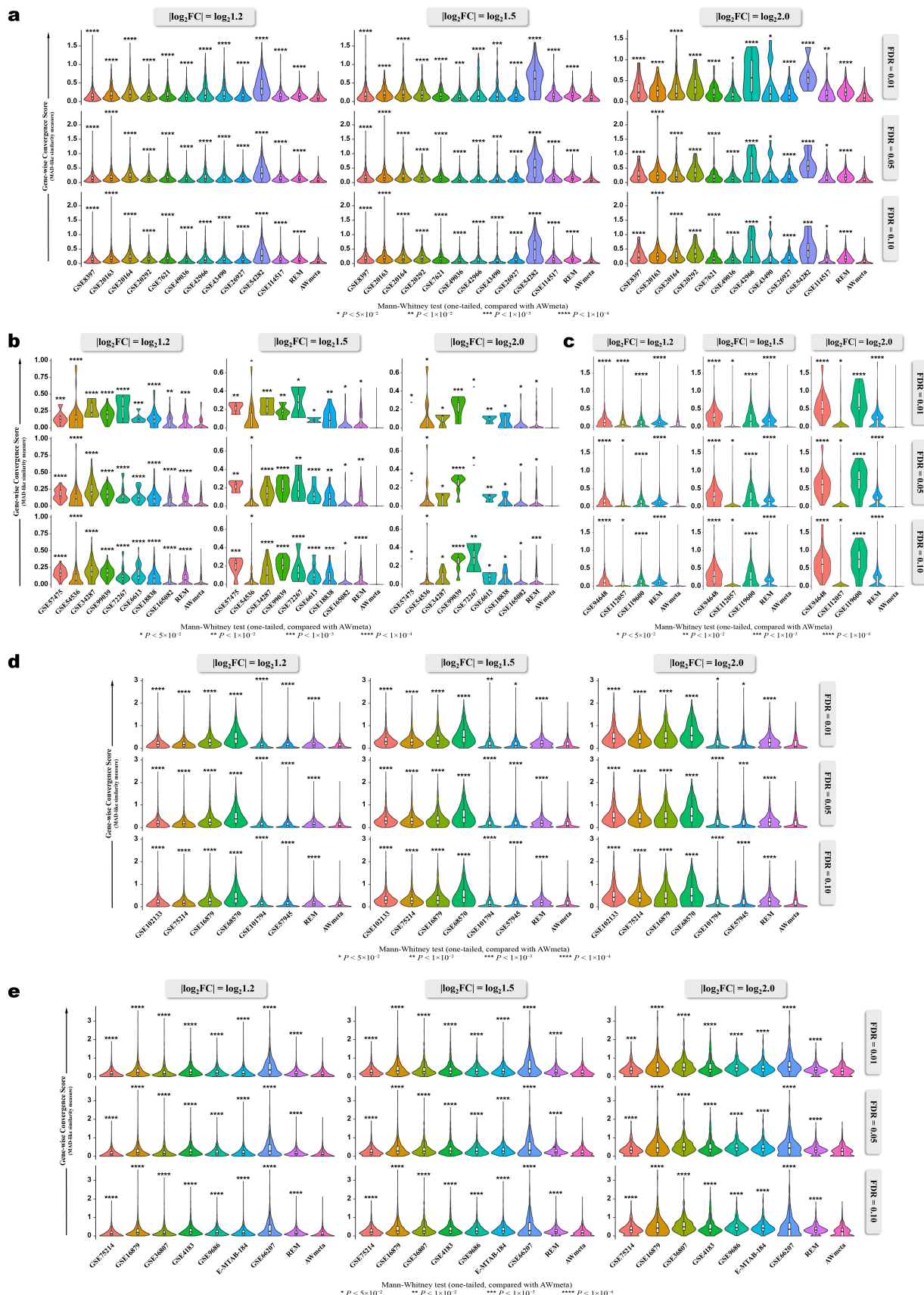


Extended Data Fig. 3 | DEG discrimination evaluation across five disease tissues using minimum-permuted semi-synthetic simulation strategy. a–e, DEG discrimination (AUROC and AUPRC) was assessed against AWmeta and REM using nine distinct thresholds, combining three corrected P -values (FDR) (0.01, 0.05, and 0.10) and three \log_2 -based fold change ($|\log_2\text{FC}|$) cutoffs ($\log_21.2$, $\log_21.5$, and $\log_22.0$), spanning Parkinson's substantia nigra (a), Parkinson's (b) and Crohn's (c) peripheral blood, and Crohn's ileal (d) and colonic (e) mucosa. Detailed description of minimum-permuted semi-synthetic simulation strategy can be referred to in "DEG discrimination evaluation using semi-synthetic simulation strategy" section in Methods, "AWmeta secures robust higher-fidelity DEG identification across transcriptomic contexts" section in Results and Fig. 1d–f. Statistical significance was determined using one-tailed Mann-Whitney test. Boxplot bounds show interquartile ranges (IQR), centers indicate median values, and whiskers extend to $1.5 \times \text{IQR}$. The following icons represent different tissue sources: 🧠: substantia nigra; 💯: peripheral blood; 🩺: ileal mucosa; 🌿: colonic mucosa.

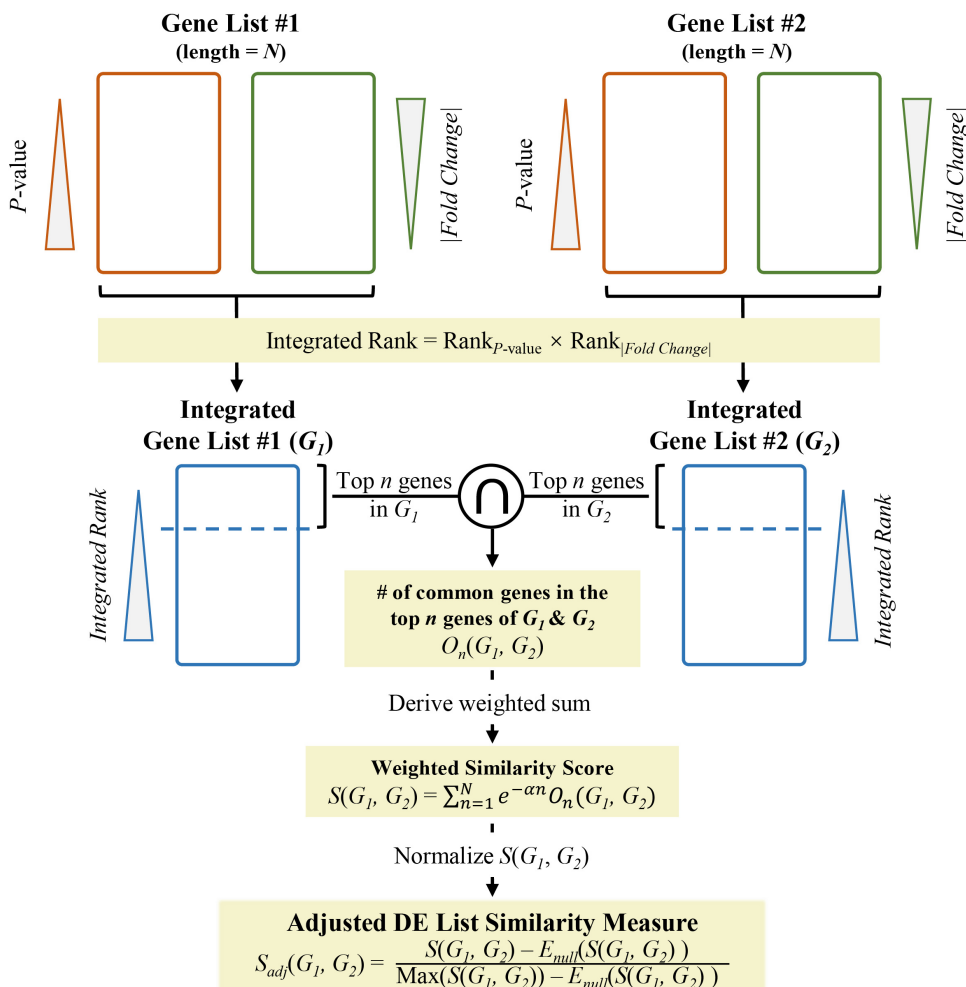




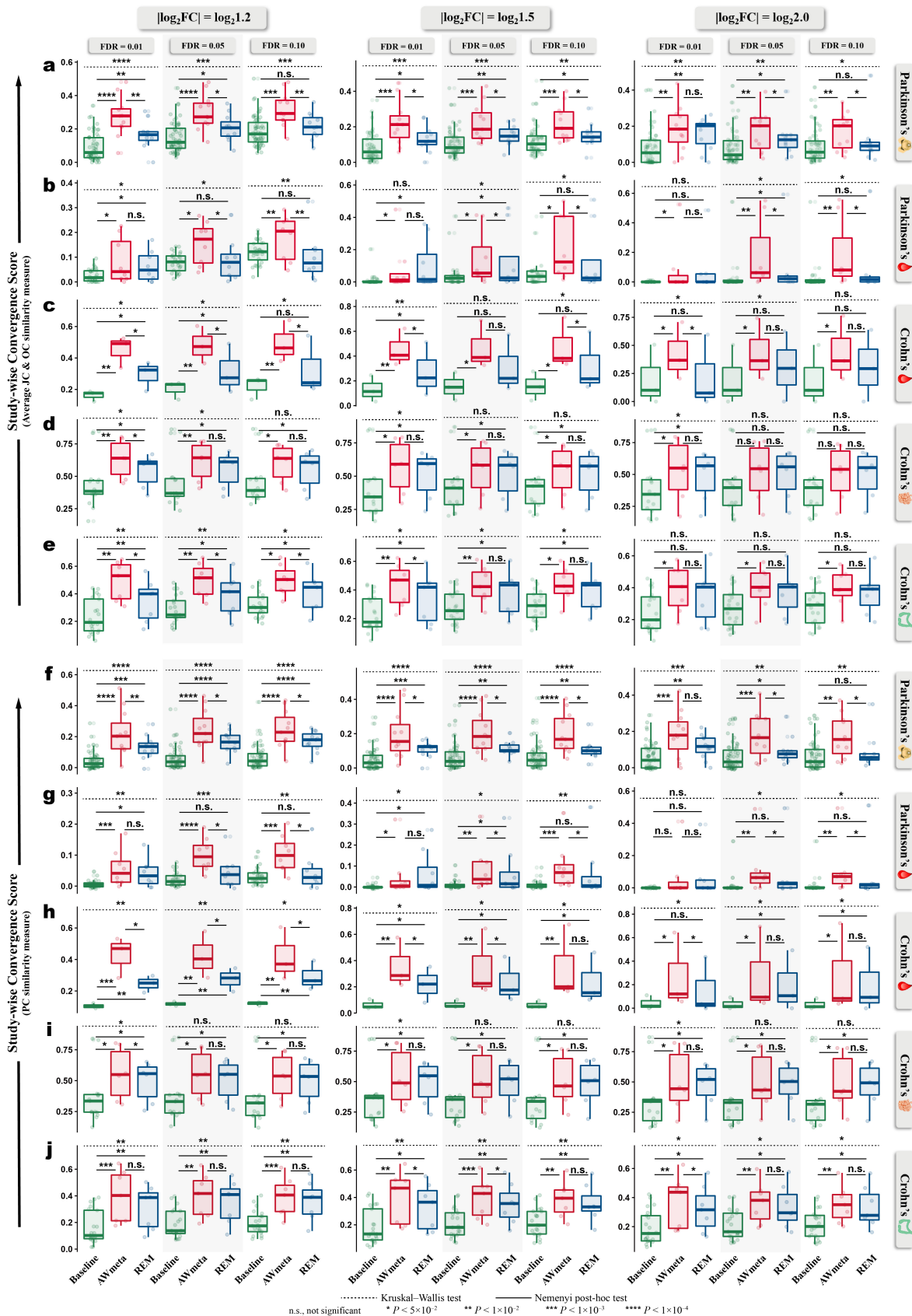
Extended Data Fig. 5 | DEG discrimination evaluation across five disease tissues using maximum-permuted semi-synthetic simulation strategy. a–e, DEG discrimination (AUROC and AUPRC) was assessed against AWmeta and REM using nine distinct thresholds, combining three corrected P -values (FDR) (0.01, 0.05, and 0.10) and three \log_2 -based fold change ($|\log_2\text{FC}|$) cutoffs ($\log_2 1.2$, $\log_2 1.5$, and $\log_2 2.0$), spanning Parkinson's substantia nigra (a), Parkinson's (b) and Crohn's (c) peripheral blood, and Crohn's ileal (d) and colonic (e) mucosa. Detailed description of maximum-permuted semi-synthetic simulation strategy can be referred to in "DEG discrimination evaluation using semi-synthetic simulation strategy" section in Methods, "AWmeta secures robust higher-fidelity DEG identification across transcriptomic contexts" section in Results and Fig. 1d–f. Statistical significance was determined using one-tailed Mann-Whitney test. Boxplot bounds show interquartile ranges (IQR), centers indicate median values, and whiskers extend to $1.5 \times$ IQR. The following icons represent different tissue sources: 🧠: substantia nigra; 💯: peripheral blood; 🍔: ileal mucosa; 🥬: colonic mucosa.



Extended Data Fig. 6 | AWmeta establishes superior DEG-wise convergence in gene differential quantification. a–e, Considering that DEGs instead of non-DEGs are primarily involved in disease etiology, to explore whether gene- (unfiltered) and DEG-wise convergence assessment results are different, mean absolute deviation (MAD)-like similarity measure was utilized to quantify the per-DEG fold change (\log_2FCI) similarity among AWmeta, REM and original studies, with smaller values indicating better convergence, which demonstrates AWmeta's consistent superior DEG- with gene-wise convergence over REM and original studies using nine distinct thresholds, combining three corrected P -values (FDR) (0.01, 0.05, and 0.10) and three \log_2 -based fold change (\log_2FCI) cutoffs ($\log_21.2$, $\log_21.5$, and $\log_22.0$), across five disease tissues: Parkinson's substantia nigra (a), Parkinson's (b) and Crohn's (c) peripheral blood, and Crohn's ileal (d) and colonic (e) mucosa. For comparison purpose, results from original studies serve as reference baselines. Statistical significance of REM and baselines against AWmeta for DEG-wise convergence comparisons was tested with one-tailed Mann-Whitney test. Detailed description for MAD-like DEG-wise convergence similarity measure can be referred to in "Gene-wise convergence assessment for gene differential quantification" section in Methods, "AWmeta establishes superior gene- and study-wise convergence in gene differential quantification" section in Results and Fig. 2a. Boxplot bounds show interquartile ranges (IQR), centers indicate median values, and whiskers extend to $1.5 \times IQR$. The following icons represent different tissue sources: 🧠: substantia nigra; 🩺: peripheral blood; 🍔: ileal mucosa; 🍔: colonic mucosa.



Extended Data Fig. 7 | Conceptual schematic of adjusted DE list similarity measure. The methodological details reside in "Study-wise convergence assessment for gene differential quantification" section in Methods.



Extended Data Fig. 8 | AWmeta maintains robust superior study-wise convergence in gene differential quantification across diverse thresholds. **a–j,** To dissect whether set-theory-based similarity-derived study-wise convergence assessment results vary with diverse DEG thresholds, we used nine distinct thresholds, combining three corrected P -values (FDR) (0.01, 0.05, and 0.10) and three \log_2 -based fold change (llog₂FCI) cutoffs ($\log_2 1.2$, $\log_2 1.5$, and $\log_2 2.0$), to benchmark study-wise convergence, which showcases AWmeta maintains robust superior study-wise convergence in gene differential quantification across diverse thresholds over REM and baselines in five disease tissues, both by means of the average of Jaccard (JC) and overlap coefficient (OC) (**a–e**) and phi coefficient (PC) (**f–j**). For comparison purpose, results from original studies serve as reference baselines. Overall study-wise convergence differences among AWmeta, REM and baselines were tested by Kruskal–Wallis test, followed by Nemenyi post-hoc test for pairwise comparisons. Details for these two study-wise convergence similarity measures appear in "Study-wise convergence assessment for gene differential quantification" section in Methods and Fig. 2h–j. Boxplot bounds show interquartile ranges (IQR), centers indicate median values, and whiskers extend to $1.5 \times$ IQR. The following icons represent different tissue sources: 🧠: substantia nigra; 💯: Peripheral blood; 🍆: ileal mucosa; 🌐: colonic mucosa.